Evidence for nuclear emissions during acoustic cavitation revisited

R I Nigmatulin[1], **R P Taleyarkhan**[2] and **R T Lahey, Jr**[3]*
[1]Institute of Mechanics, Ufa-Bashkortostan Branch, Russian Academy of Sciences, Ufa, Russia
[2]Department of Mechanical Engineering, Purdue University, West Lafayette, Indiana, USA
[3]Center for Multiphase Research, Rensselelaer Polytechnic Institute, Troy, New York, USA

Abstract: This paper extends the experimental and numerical results presented previously and addresses the major criticisms raised. In addition, the most recent results are discussed. In acoustic cavitation experiments with chilled ($\sim$0 °C) deuterated acetone (C_3D_6O), the production of tritium and 2.45 MeV neutrons [which are characteristic of deuterium-deuterium (D–D) fusion] was observed during vapour bubble implosions in an acoustic pressure field. Similar experiments with deuterated acetone at room temperature ($\sim$20 °C) and control experiments with normal acetone (C_3H_6O), at both 0 and 20 °C, showed no statistically significant increases in either tritium level or neutron emissions. Numerical simulations of the processes that account for the shock waves generated in the liquid and within the collapsing bubbles supported these experimental observations and showed that high densities and temperatures ($\geqslant 10^8$ K) may be achieved during bubble cloud implosions, yielding the conditions required for D–D nuclear fusion reactions. The present paper treats the bubble fusion experiments and theoretical results in greater detail than was possible in the previous publications, contains some refinements, addresses some important questions raised by reviewers and critics and discusses possible applications of this interesting phenomenon.

Keywords: sonofusion, cavitation bubble dynamics

1 INTRODUCTION

The purpose of this paper is to extend and enhance the experimental and numerical results on bubble fusion presented previously in *Science* [**1**] and *Physical Review—E* [**2**] and to address the major criticisms raised. This discovery generated significant media coverage and discussion in the scientific community, some of which was sceptical of the claims made. It should be noted that some of the critics incorrectly assumed that bubble fusion was just another form of 'cold fusion'. As will be explained in this paper, this is completely incorrect. First of all, some of the background that led to the discovery of bubble fusion (i.e. sonofusion) will be summarized.

The intense implosive collapse of gas and/or vapour bubbles, including acoustically forced cavitation bubbles, can lead to ultrahigh compressions and temperatures and to the generation of light flashes attributed to sonoluminescence (SL) [**3**–**16**]. The basic physical phenomena associated with single-bubble sonoluminescence (SBSL) are shown schematically in Fig. 1. The bubbles typically oscillate in an impressed acoustic pressure field (i.e. a standing wave). During the rarefaction phase they grow, and during the compression phase they rapidly collapse (i.e. implode). Figure 1a shows the start of bubble implosion when the gas Mach number ($M_g \equiv \dot{R}/C_g$) based on interfacial velocity, $\dot{R}$, is much less than unity. As the interfacial Mach number approaches unity, a compression shock wave is formed in the gas/vapour mixture and, as shown schematically in Fig. 1b, this shock wave (dashed line) moves towards the centre of the bubble and, in doing so, intensifies.

Figure 1c shows the situation just after the shock wave has bounced off itself at the centre of the bubble which highly compresses and heats a small core region near the centre of the gas/vapour bubble. At this point there is normally an SL light pulse, and, if the composition of the vapour/plasma and the resulting temperatures, density and their duration are large enough, there may also be conditions suitable for nuclear emissions (i.e. nuclear fusion). Interestingly, the pressurization process continues until a short time

The MS was received on 6 June 2003 and was accepted after revision for publication on 14 May 2004.

**Corresponding author: Rensselaer Polytechnic Institute, Troy, New York 12180, USA.*

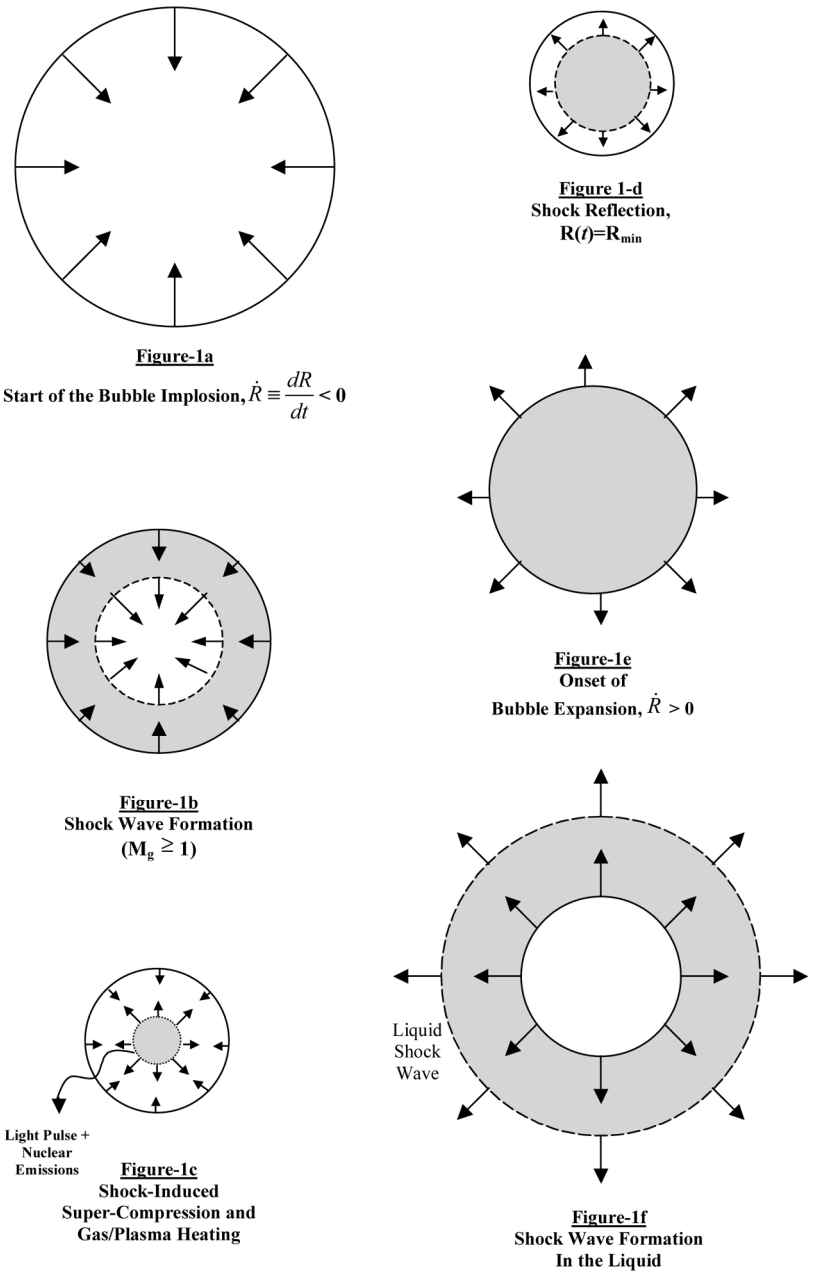

Fig. 1 Schematic of sonoluminescence and bubble fusion phenomena

later (i.e. $\leqslant 10^{-12}$ s) when the interface comes to rest (see Fig. 1d).

Figure 1e shows the onset of bubble expansion during the reflection phase of the impressed acoustic pressure field, and Fig. 1f shows that a relatively weak shock wave is formed in the liquid surrounding the bubble during bubble expansion. This shock wave is easily heard by the experimenters as it reaches the wall of the test section in which the experiment is being performed. There is extensive literature on sonoluminescence (e.g. reference [**17**]) and thus this interesting phenomenon will not be discussed at great length in this paper. Rather, the focus will be upon bubble fusion technology.

2 LESSONS LEARNED FROM SONOLUMINESCENCE EXPERIMENTS AND ANALYSIS

It is impossible to make direct experimental measurements of the highest temperatures achieved during sonoluminescence, since for high temperatures (i.e. above 10^4 K) the electromagnetic emissions corresponding to these temperatures (or, more precisely, to the temperature of the electrons radiating photons owing to electron dynamics) are absorbed by the optically opaque dense gas core in the bubble and, depending on the wave length of these emissions, in the first

few millimetres of the liquid. Rather, the peak temperatures achievable during sonoluminescence must be inferred from fitting the emission spectrum [**18**] or from detailed calculations. The SBSL emission spectrum from oscillating small xenon gas bubbles in water at high frequency (1 MHz) was fitted to a thermal bremsstrahlung spectrum and indicated 10^6 K plasma temperatures [**18**]. Also, Moss *et al.* [**19**–**21**][†] performed calculations for the spherically symmetric implosion of a gas bubble in acoustic fields with frequencies of 27 and 45 kHz, and liquid pressure amplitudes near the bubble of either 0.25 bar or 1.5 bar. These conditions are typical of single-bubble sonoluminescence (SBSL) experiments, when the bubble grows from an initial radius of about $R_0 = 4.5$ μm (or 10 μm), when in equilibrium with the average pressure in the fluid, to about 40 μm (or 80 μm) during the acoustic rarefaction phase, and then implodes to a radius of about 0.3 μm (or 3 μm) during the acoustic compression phase. Significantly, the final stage of collapse is only about $\sim 10^{-3}$ μs = 1 ns in duration. During bubble implosion, a shock wave is initiated within the bubble because of the fluid acceleration towards the centre of the bubble. While focusing (i.e. cumulating) towards the centre of the bubble and then bouncing back, the shock wave compresses the gas (owing to the inertial forces in the fluid accelerated towards the centre) and heats it up to high temperatures. When the shock wave is focused at the centre, a high-density ionized gas/vapour core is produced near the bubble centre. According to Moss' calculations, this plasma core has a radius, r_*, a lifetime of the highly compressed state (before dissipation), Δt_*, a maximum gas/plasma density, ρ_*, a peak pressure, p_*, and a peak ion temperature, T_{i*}, of the following approximate values

$$r_* \sim 10^{-9}\,\text{m}, \quad \Delta t_* \sim 10^{-11}\,\text{s}, \quad \rho_* \sim 10\,\text{g/cm}^3, \quad p_* \sim 10^9\,\text{bar}, \quad T_{i*} \sim 10^6\,K \tag{1}$$

Significantly, the electron temperature, T_{e*}, required for sonoluminescence (SL) was about 3 times less.

The assessment [**20**] of the possibility for nuclear fusion to occur under the stated conditions for a bubble containing a deuterium–nitrogen mixture (nitrogen was added to slow down the sound speed in the gas) gave a very small rate of neutron production equalling about 10^{-1}/h, which corresponds to only 10^{-5} neutrons per implosion (the invalid points in the calculations stated previously can lead to a reduction in the D–D fusion neutron production rate by a factor of 10–100, and thus, for the conditions analysed, the predicted neutron production rate would be negligible). Nevertheless, these calculations gave a very important result—namely the predicted duration of an SL light flash, determined by the lifetime of the highly compressed hot central core (10^{-11} s), was in good agreement with experimental measurements of the duration of SBSL light flashes. This implied that shock-induced compression heating occurred during bubble implosions.

It should be kept in mind that such an abnormally high heating of a tiny central zone in the bubble occurs at the expense of transforming into internal energy a part of the kinetic energy of the fluid accelerated towards the bubble centre. The greater the kinetic energy, the higher will be the compression and heating of the central gas/vapour core region.

The aim of the experiments previously published in *Science* [**1**] was to reach intense heating that was at least 2 orders of magnitude higher (i.e. up to 10^8 K) than in typical SBSL experiments, creating conditions suitable for nuclear fusion. For this purpose, a novel experimental procedure was applied that enabled a large increase in the kinetic energy of the fluid accelerating towards the bubble centre and thus enhanced the effect of the cumulative shock wave compression of the central core region of the imploding bubble.

In particular, use was made of much greater amplitudes of the acoustic field than the conventional 1.0–1.5 bar amplitudes used in SBSL experiments which were limited on account of rectified diffusion, inherent shape and interfacial instabilities and a reversal in the sign of the Bjerknes force [**23**]. In particular, relatively intense harmonic acoustic fields having an amplitude of 15 bar or more (i.e. 15–40 bar) were imposed. To do this, two difficulties had to be surmounted. The first was to choose a liquid that could accommodate repetitive high-frequency states of tension without premature cavitation. The second was to develop and focus intense acoustic fields in a rather small zone within the liquid; this required the use of a different experimental technique [**24**, **25**] than used in SBSL experiments.

Moreover, instead of a non-condensable gas bubble (as used in SBSL experiments), vapour cavitation bubbles were used (i.e. the bubbles were filled with vapour of the surrounding deuterated liquid). The problem was that the fluid being accelerated towards the bubble centre was cushioned by the increasing gas pressure caused by the fluid-induced gas compression. In contrast, in a vapour bubble the effect of cushioning is mitigated owing to vapour condensation at the bubble interface (i.e. during bubble compression some of the vapour is condensed into liquid). When compressing a non-condensable gas bubble of constant mass, its pressure grows. In contrast, the pressure of an imploding vapour

[†]It should be noted that some points of the investigations reported by Moss *et al.* are invalid. In particular, as shown in the paper by Nigmatulin *et al.* [**22**], the adiabatic state of the gas assumed in their calculations was in error. Actually, the gas remains isothermal for almost the whole period of bubble expansion and compression and its temperature is essentially the same as in the liquid pool. It is not difficult to show that during the 30–50 μs long period of bubble oscillations, thermal waves have a chance to equalize the gas temperature in a bubble of ~50 μm radius to that of the surrounding fluid. Only during the final stage of the implosion (which is about 10^{-9} s = 10^{-3} μs long), when the radius decreases from about $2–3R_0$ to its minimum, R_{min}, with an interface velocity of $\sim 10^3$ m/s, will there be adiabatic gas heating. As a result, the thermal cycle of the bubble corresponds to a thermal pump cycle. In addition, Moss only calculated the very first oscillation after rest and not the steady state oscillations, when the amplitude, fluid kinetic energy and temperature achieved in the hot nucleus are several times higher than those for the first implosion. Nevertheless, his basic conclusions were correct.

bubble remains almost constant in time owing to vapour condensation until the final phase of collapse. This mitigates the effect of gas/vapour cushioning during bubble implosion.

In the present bubble fusion experiments [**1**, **2**] the vapour bubbles were nucleated at the point of maximum liquid tension by using energetic neutrons which collided with the atomic nuclei of the liquid. The nucleation centres of the bubbles had an initial radius, R_0, of $\sim 0.01-0.1$ μm, and these bubbles grew rapidly during the phase of fluid rarefaction induced by an acoustic pressure field and reached a maximum radius $R_m \approx 500-800$ μm, which was an order of magnitude greater than in typical SBSL experiments (where, $R_m \approx 50-80$ μm). Thus, in the present experiments, the maximum bubble volume was larger by a factor of three orders of magnitude in comparison with typical SBSL experiments. Because of the previously mentioned reduced cushioning owing to vapour condensation, the order of magnitude higher compression pressure of the acoustic field and the larger maximum bubble volume, the liquid near the vapour bubble interface was accelerated towards the centre at much higher radial velocity, w (i.e. up to about 7 km/s). As a result, the kinetic energy of the fluid, determined by the product $R^3\dot{R}^2$, was about 10^4 times higher than the kinetic energy in typical SBSL experiments. Moreover, this energy was imparted not to the total amount of vapour that filled the bubble at the instant of its maximum size but only to the vapour left after condensation had taken place. The present analysis indicates that, depending on the conditions being analysed, 50–90 per cent of the vapour is condensed (i.e. by the time of maximum compression there is only 50–10 per cent of the vapour left in the bubble relative to the vapour mass at the time of maximum bubble size). Thus, in the present experiments, the vapour left by the time of bubble collapse is about 100 times (but not 1000 times) more than in typical SBSL experiments. As a result, there was $10^4/10^2 = 100$ times more fluid kinetic energy imparted to a unit mass of vapour/plasma in the present bubble fusion experiments [**1**, **2**] than in typical SBSL experiments.

Thus, if the gas ion temperature during SBSL experiments was $T_{i*} \sim 10^6$ K, in the present experiments using cavitation-induced vapour bubbles, the ion temperature would be expected to reach $T_{i*} \sim 10^8$ K, which implies conditions suitable for D–D nuclear fusion. The influence of the maximum bubble size, R_m, determined by the amplitude of acoustic forcing and the interfacial implosion rate, w, on higher gas compression was also supported by independent experiments [**16**, **26**]. In particular, it was noted in these experiments that increasing R_m modestly (by ~50 per cent), or increasing the rate of collapse, w, resulted in very large increases in light emission during bubble implosion.

3 CHOICE OF THE TEST LIQUID

Given the present objectives, the authors elected to work with an organic liquid. Acetone was chosen (density $\rho_L = 0.79$ g/cm^3, sound velocity $C_L \approx 1190$ m/s), and it was degassed so that it was free from non-condensable gases in the liquid. There were two isotopic compositions used: normal acetone (C_3H_6O, hereafter called H-acetone) was the control fluid, which, in practice, is without nuclei capable of undergoing nuclear fusion, and deuterated acetone (C_3D_6O, hereafter called D-acetone) was the primary test fluid. Significantly, D-acetone contains deuterium (D) nuclei which are capable of undergoing nuclear D–D fusion reactions at sufficiently high temperatures and densities.

There were a number of reasons for the choice of acetone:

1. Deuterated acetone is easily available and of relatively low cost. Also, it has a high cavitation strength (i.e. it permits the attainment of large tensile states without premature cavitation). This, in turn, permits large values of liquid superheat to be attained, and thus rapid evaporation rates and large maximum bubble sizes subsequent to nucleation.
2. In the vapour phase of acetone (the molecular weight of D-acetone is 64) the sound velocity is relatively low. Thus, a fixed interface velocity compressing the bubble results in the formation of strong shock wave compressions.
3. Organic liquids have relatively large accommodation coefficients for condensation. As will be described later, it is very important to have intense condensation during implosive bubble collapse. Certainly, the presence of foreign atoms or nuclei (i.e. four nuclei and 52 g of carbon and oxygen out of ten nuclei in 64 g of acetone respectively) leads to losses in energy owing to carbon and oxygen ion heating and poses impediments to D nucleus approach and collision. Nevertheless, the advantage of a large accommodation coefficient and relatively low speed of sound far outweighs these losses.

Unless otherwise noted, the liquid in the acoustic chamber was maintained at ~0 °C, which was the lowest value obtainable with the equipment that was used in the present experiments [**1**, **2**]. The test liquid was degassed and subjected to an acoustic pressure field that oscillated at the resonance frequency of the liquid sample in the test section (i.e. a standing acoustic wave having a single pressure antinode was formed).

4 EXPERIMENTAL SYSTEM

As shown schematically in Fig. 2, the basic experimental apparatus used in the present experiments was a cylindrical test section made of Pyrex (i.e. borosilicate glass) that was 65 mm in diameter and 20 cm in height. The test section (i.e. acoustic chamber) was filled with the test liquids (i.e. degassed D- or H-acetone), and a lead zirconate titanate (PZT) piezoelectric transducer ring was attached to the outer surface with epoxy.

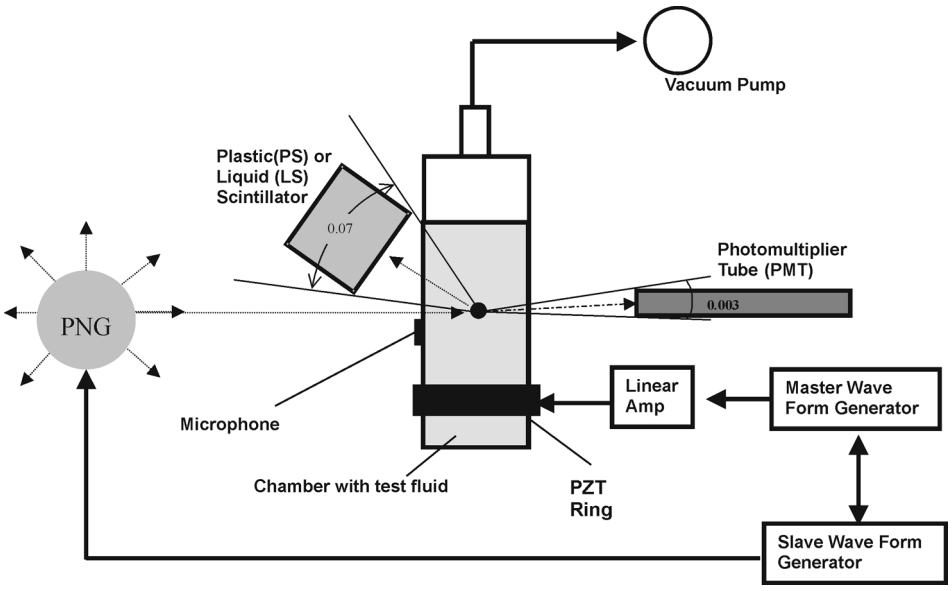

Fig. 2 Experimental set-up. The distance from the scintillator head (PS or LS) to the PNG is ~15 cm, from the scintillator head to the chamber surface 0–2 cm, from the chamber centre to the PNG ~20 cm and from the PMT to the chamber surface ~5 cm. The system (i.e. the chamber, PNG and PMT) was ~1.5 m above the floor [**1**,**2**]

This test section was designed, manufactured and operated at the Oak Ridge National Laboratory (ORNL) for the bubble fusion experiments previously reported [**1**, **2**]. The flask walls and the liquid within were harmonically driven with the PZT. The acoustic frequency was $f = 19.3$ kHz, with an acoustic period of about 52 μs. The acoustic chamber under consideration was a high-Q acoustic system and, as such, required careful tuning for optimal performance (i.e. to achieve about 30–50 implosions per second) during the bubble cloud implosions. To detect the shock waves caused by the bubble cloud implosions, two pill microphones were installed on diametrically opposite outer sides of the chamber.

All experiments were conducted in the test section shown schematically in Fig. 2 using H-acetone (100 at % pure C_3H_6O) and D-acetone (99.92 at % C_3D_6O), which were initially filtered through a 1 μm filter. Degassing was performed at vacuum conditions (~10 kPa), and acoustic cavitation of the liquid was performed for about 2 h to promote the removal of non-condensable gases from the liquid.

Nucleation of the vapour bubbles was initiated with fast neutrons from either an isotopic source (Pu–Be) or a pulsed neutron generator (PNG), which was fired on demand at a predefined phase of the acoustic pressure field. The Pu–Be source produced neutrons at a rate of $\sim 2 \times 10^6$ n/s. In this case most of the neutron energy was below 5 MeV (i.e. 75–80 per cent), and about 10 MeV was the maximum energy emitted.

The PNG generated 14.1 MeV neutrons at a rate of $\sim 5\text{–}6 \times 10^5$ n/s and it was operated at a frequency of 200 Hz (i.e. ~2500–3000 neutrons per pulse). Each PNG neutron pulse was about 12 μs in duration and was phase matched with acoustic pressure oscillations. In particular, the PNG was fired during the liquid expansion phase when pressure achieved its minimum (negative) value. As follows from the given acoustic (19.3 kHz) and PNG (200 Hz) frequencies, the PNG neutron pulse was produced not in each acoustic cycle but once per ~100 acoustic oscillations. The reason for using a pulse neutron source with relatively low frequency for initiating cavitation was to minimize the background due to the 14.1 MeV PNG neutrons when 2.45 MeV neutron emissions were produced during bubble implosions.

Either a plastic (PS) or a liquid (LS) scintillation detector (i.e. scintillator) was used for detection of the neutron and gamma signals. The Bicron BC404 PS had dimensions of 5 cm (diameter) × 2.5 cm (thickness) and the Elscint LS had dimensions of 5 cm (diameter) × 5 cm (thickness) [**1**].

For the LS, pulse-shape discrimination (PSD) was used [**27**–**30**]. This technique made it possible to count neutrons separately from gamma ray induced scintillations on the basis of differences in the signal decay time of each type of scintillation. The discrimination of neutron scintillations was important since it made it possible to determine the energy of each neutron-induced scintillation, or, more precisely, the energy of the recoil proton responsible for the given scintillation. When striking a proton, each neutron, of energy E_n, gives up some of its energy to a proton in the LS. The energy of this proton (called a recoil proton), E_p, will thus be in the range $0 \leqslant E_p \leqslant E_n$. Hence, the 2.45 MeV D–D neutrons that were measured by the LS registered an energy of less than or equal to 2.45 MeV.

The LS detector was calibrated *in situ* with cobalt-60 and cesium-137 gamma ray sources by relating the Compton

edge of each spectrum to the energy of the proton that would produce the same amount of light in the scintillator [**27**, **29**]. Using a multichannel pulse height analyser (MCA) with 256 channels, the energy of a 2.45 MeV proton was determined to lie near channel 40; in particular, in the measurement system reported on in *Science* [**1**], a 2.45 MeV neutron had a proton recoil 'edge' at channel 32. Similarly, measurements with the 14.1 MeV PNG neutrons showed a proton recoil edge near channel 110 (i.e. channel 115). Subsequent analysis of these results showed that there was a 21-channel offset in the MCA such that zero energy corresponded to channel 21. Thus, 21 channels must be subtracted from the pulse height data before comparing energies of Compton and proton recoil edges. Doing this, the ratio of 14.1 to 2.45 MeV neutrons was $(115-21)/(32-21) \sim 9$, which is consistent with previously reported values [**27**, **29**, **31**].

The efficiency of the Elscint LS used [**1**], designated as η_{ET}, was determined using a Pu–Be neutron source with a known intensity of $\sim 2 \times 10^6$ n/s. By positioning the source near the face of the LS detector (i.e. at a distance of ~ 1 cm), the efficiency of this detector was found to be $\sim 5 \times 10^{-3}$. This was corrected for the true distance (5–7 cm) between the LS and the 2.45 MeV neutron source (i.e. the zone of cavitation) in the present experiments and also for the corresponding solid angle (see Fig. 2), giving an estimated efficiency that was less by a factor of from $(5/1)^2 = 25$ to $(7/1)^2 = 49$. When estimating the neutron production in the zone of cavitation, it should also be noted that about 50 per cent of the 2.45 MeV neutrons are attenuated in the acetone-filled flask, so the efficiency of neutron detection (the correction for neutron losses in the liquid-filled flask was made after the publication in *Science* [**1**]) from the zone of cavitation in the present measuring configuration (Fig. 1) was

$$\eta_{ET} \sim 5 \times 10^{-3} \times (0.02–0.04) \times 0.5 = (0.5–1) \times 10^{-4} \quad (2)$$

The 'light signals' (i.e. the actual SL light pulses from the cavitation zone and the flashes occurring owing to the interaction of neutrons and gamma rays with the PMT) were detected in a Hammamatsu R212 photomultiplier tube (PMT), which had a 2 ns rise time [**1**]. The timing of the SL light flashes relative to the PS or LS nuclear-induced scintillations was made using a multichannel analyzer (MCA) and a high-speed digital storage scope.

5 DESCRIPTION OF THE PROCESS

To ensure robust nucleation and significant bubble growth and implosions, the drive voltage to the PZT was set to be at least double that needed for the initiation of neutron-induced cavitation in the acetone in the test section. The negative pressure threshold for bubble nucleation by neutrons and alpha particles in acetone is -7 to -8 bar [**32**, **33**]. A pressure map of the liquid in the acoustic chamber was obtained using a calibrated hydrophone. Using the measured linear scale factor for the induced pressures in the present chamber versus drive voltage to the PZT, and gradually increasing the drive amplitude of the acoustic field pressure, it was verified that neutron-induced acoustic cavitation began at a negative pressure in the test section of about -7 bar. In the bubble fusion experiments under consideration [**1**] the pressure amplitude within the zone of bubble cluster nucleation was $\geqslant 15$ bar. The sequence of events shown schematically in Fig. 3 will now be considered.

A 14.1 MeV neutron pulse from the PNG induces cavitation in the liquid at the position in the chamber axis where the acoustic pressure antinode is located and at the instant when the liquid at that position is under significant tension. At this time, the neutron scintillator (PS or LS) detects, as expected, the neutron pulse from the PNG. The interaction of 14.1 MeV neutrons with the tensioned liquid gives rise to the nucleation of visible bubble clouds (occurring at a rate of $\sim 30–50$ per second), and photographic evidence indicates that the bubble clusters that are formed consist of about 1000 microbubbles [**1**]. During rarefaction conditions these microbubbles grow rapidly with the bubble cluster until the increasing acoustic pressure in the liquid during the second half of the acoustic cycle arrests their growth and causes them to begin to collapse, resulting in an implosion. If the implosion is robust enough, the bubbles emit SL light flashes, which can be detected by the PMT. The Rayleigh equation for an inviscid incompressible liquid shows that, if the pressure in a bubble does not increase during compression (e.g. owing to intense vapour condensation with the remaining vapour being uncompressed), the speed of the liquid at the bubble interface tends to infinity. At some point in time, however, the rate of condensation will not be able to compensate for the bubble volume reduction, and, from this time on, the remaining vapour will begin to be compressed and grow in pressure. When the liquid speed at the interface approaches the speed of sound in the vapour, the liquid, as if it were a piston, will generate compressive shock waves in the vapour directed towards the bubble centre. These waves, focusing and concentrating at the bubble centre and reflecting from it, induce, in the remaining non-condensed vapour core, ultrahigh temperatures, pressures and densities for a very short period of time. If the vapour contains deuterium (D) and/or tritium (T) atoms, and the temperature and vapour/plasma density in the highly compressed core near the bubble centre are high enough for a sufficiently long time interval, then D–D (and/or D–T) fusion can occur in addition to the SL flash. As a result, nuclear particles (i.e. neutrons, protons, He, T nuclei and gamma rays) will be produced. The emitted neutrons and gamma rays will be detected owing to their collisions with the nuclei (protons) in the PS or LS scintillator.

The zone of high pressure, density and temperature that is produced as a result of the imploding bubble causes the

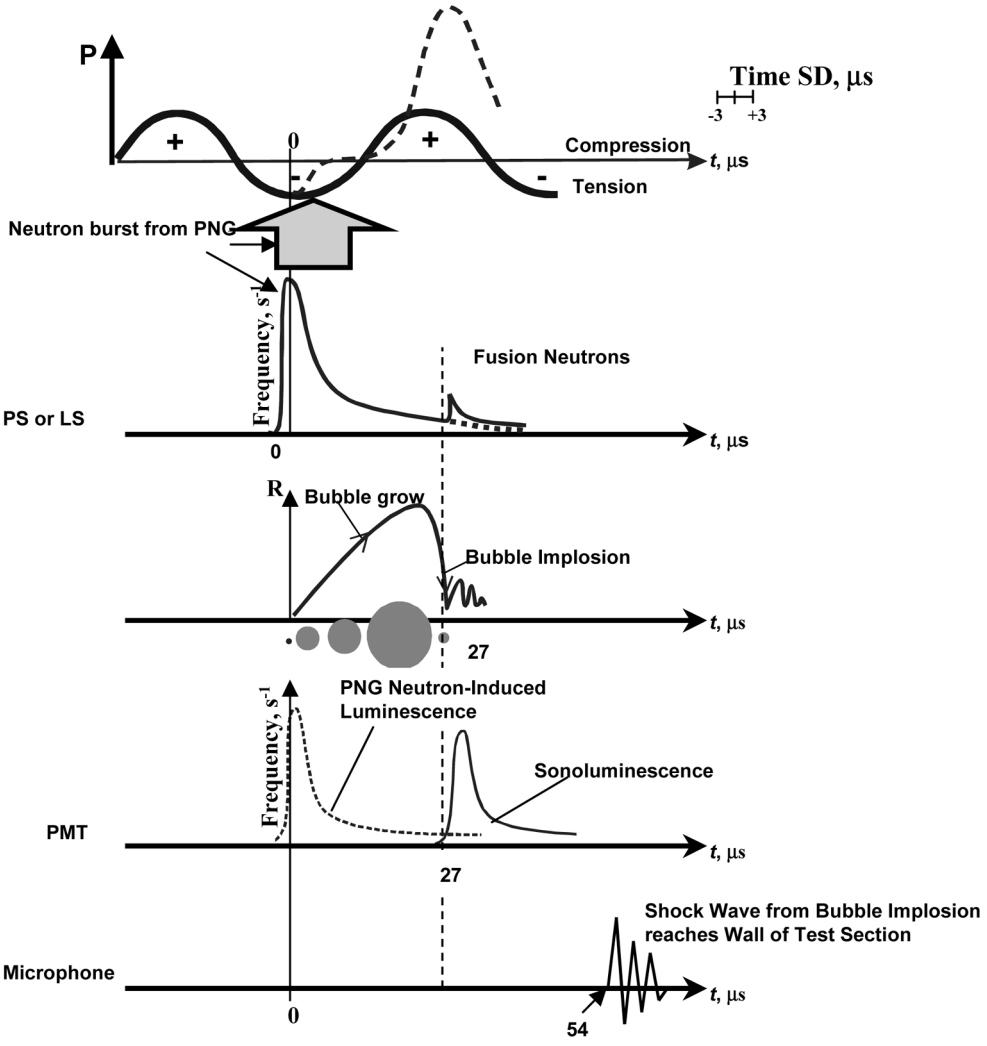

Fig. 3 Experimental sequence of events

generation of a reflected shock wave radiating outwards from the bubble centre. This relatively weak shock wave subsequently travels in the liquid at about the speed of sound and is easily detected at the test section walls with pill microphones.

6 TIMING OF KEY PARAMETERS

The electronic timing system ensures accurate determination of the moment of greatest tension of the liquid (i.e. the maximum negative acoustic pressure) in the acoustic antinode on the flask axis. This time instant (see Fig. 3) may be taken as the starting point for the time reference ($t = 0$). Just before this time instant (i.e. at $t \sim -2\ \mu s$), a neutron 'burst' was initiated in the PNG. Some of the neutrons from this short isotropic burst make it to the acoustic antinode. When analysing the time spectrum of the neutrons from the PNG, it was found that most of the neutrons were emitted over the interval $t \approx -2\ \mu s$ to $t \approx 10\ \mu s$ (which corresponded to a PNG pulse full width at half-maximum of about 6 μs). The pressure amplitude at the antinode was more negative than that required for threshold nucleation. Hence, because of the PNG pulse, bubble nucleation could occur at $t = -2\ \mu s$ and persist for $t > 0$ (i.e. somewhat after the minimum liquid pressure was reached). Nevertheless, the effect of the PNG neutrons was negligible by the time ($\sim 27 \pm 3\ \mu s$) that D–D neutrons were produced during implosion of the bubbles. In any event, as shown schematically in Fig. 3, a cluster of cavitation microbubbles was nucleated by the PNG neutrons in the tensioned liquid at the acoustic antinode. As discussed previously, and as shown in Fig. 3, these microbubbles grew rapidly owing to the negative acoustic pressure {as shown schematically in Fig. 3 (dashed line), owing to rapid evaporation immediately after the bubbles are nucleated, the liquid pressure surrounding them rapidly approaches the saturation pressure, after which it increases significantly as a result of bubble cluster dynamics [**34**, **35**]}, and their maximum radius reached $R_m \sim 500-800\ \mu m$. When the liquid pressure around the bubble cluster became positive, the bubbles imploded, undergoing compression heating of the

uncondensed vapour remaining in the imploding bubbles. During implosion of the various bubbles, SL light flashes are emitted from the cluster of bubbles. The initial SL flash due to the first bubble collapse takes place at $t_{1C} = 27 \pm 3$ μs (see Fig. 3). Other SL flashes (from other bubbles within the cluster) were observed during the subsequent 15 μs interval, with the highest intensity within the first 5 μs. Measurements using a different detection system [**36**] showed secondary SL and gamma ray signals being emitted much later and over a much longer time span (i.e. from 500 to 2500 μs), the total number of such secondary SL and gamma ray signals being greater than that during the initial implosion. This implies that there were subsequent acoustically driven bubble cluster implosions (i.e. bounces). Subsequent experiments reported in *Physical Review—E* [**2**] have confirmed and extended these data trends and have shown that not only are SL and gamma rays produced after the initial implosion of the bubble cloud but also 2.45 MeV D–D neutrons. These data are shown in Fig. 4, from which it can also be seen that there was strong coincidence between the D–D neutron emissions and the SL light flashes for chilled, cavitated D-acetone [**2**].

As shown schematically in Figs 1 and 3, bubble implosions result in a shock wave being reflected from the bubble centre, and the resultant pressure pulse in the liquid reaches the flask wall at $t_{1W} = 54 \pm 3$ μs (see Fig. 3). This impulsive pressure signal was recorded by two pill microphones installed on opposite sides of the test section wall. The time for a shock wave to travel from the centre of the chamber to its walls (about 32 mm away) was $t_{1W} - t_{1C} \approx 27$ μs, which is in agreement with the fact that a shock wave travels in the liquid (acetone) at about the speed of sound, $C_L \approx 1190$ m/s.

Because the high-energy PNG neutrons were emitted in all directions (i.e. over a 4π solid angle), they did not always reach the pressure antinode in the test section. Thus, the production rate of bubble clouds was several times less than the frequency of the neutron pulses from the PNG, and the implosion rate varied from ~30 to 50 implosions per second, depending on PZT excitation tuning. Moreover, subsequent to each bubble cloud implosion, shock wave excitation of the flask walls and the resultant defocusing of the acoustic standing wave lasted for about ten acoustic cycles (~520 μs). During this time the coherent standing acoustic wave, and thus the cavitation process, was disturbed.

The time spectrum of the above-mentioned events showed that the initial PS or LS scintillations corresponding to the PNG activation (lasting about 12 μs) was followed by SL flashes (lasting about 15 μs) which started about 27 μs later. As noted previously, the PNG neutrons were emitted

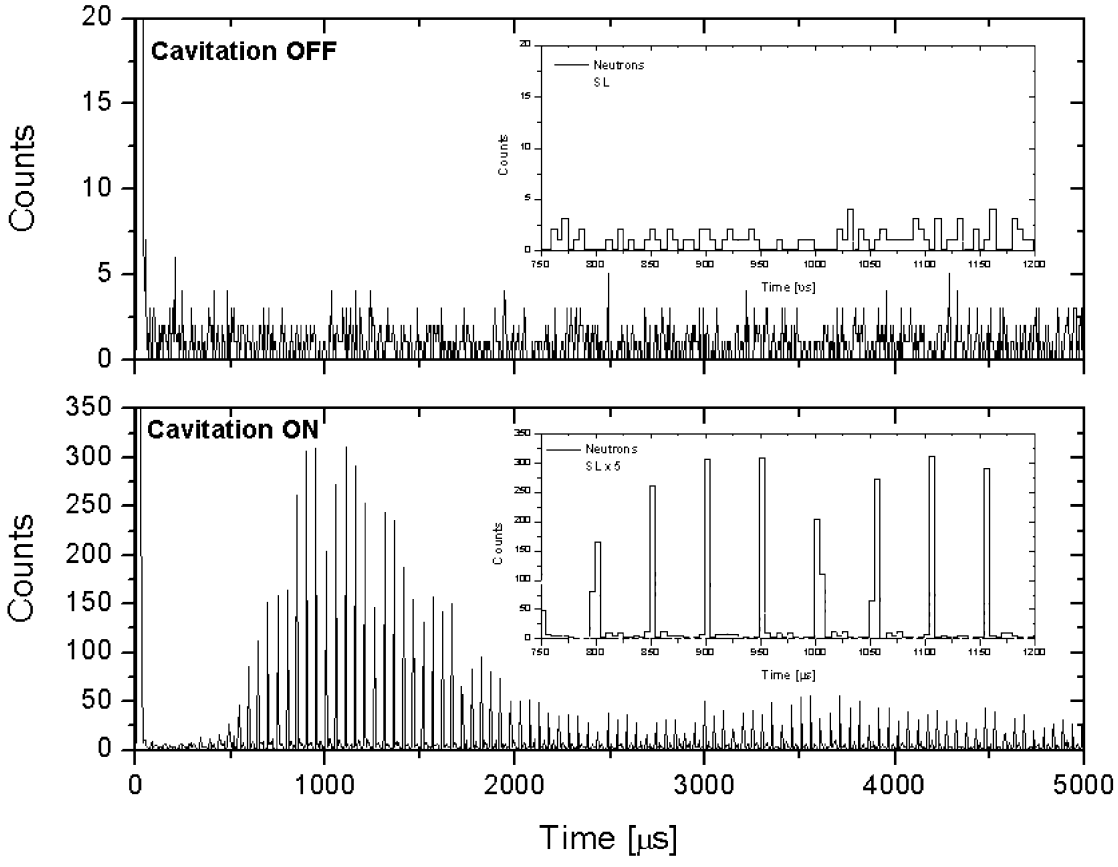

Fig. 4 Data for chilled, irradiated C_3D_6O with and without cavitation [**2**]

isotropically (i.e. over a 4π solid angle). Moreover, those that went in the direction of the pressure antinode may collide with the atomic nuclei in the liquid and the apparatus and structures around it, thus losing some of their energy. Some of them reached the scintillator directly and produced successively less frequent LS scintillations for $\sim$20 μs. Anyway, the primary neutrons from the PNG created a relatively high neutron background for several tens of microseconds. Because of this, it was necessary to separate the scintillations from the primary (PNG) and secondary neutrons (generated by D–D fusion). To achieve this, the former were fired for only a short period ($\sim$12 μs), at a frequency that was 100 times less than that of the pressure acoustic field (i.e. at 200 Hz). Since the PNG neutron level was essentially at background about 20 μs after the PNG burst, the D–D neutrons shown in Fig. 4 were well separated in time from the PNG neutrons, and this continued over a 5000 μs interval before the PNG was again fired.

7 EVIDENCE OF NUCLEAR FUSION

Each D–D fusion event can lead to one of two almost equally probable nuclear reactions. These are:

(a) the production of a 1.01 MeV tritium (T) nucleus and a 3.02 MeV proton;
(b) the production of a 0.82 MeV helium-3 (He) nucleus and a 2.45 MeV neutron.

The evidence that D–D fusion occurred during the implosion of cavitation vapour bubbles in chilled D-acetone includes:

(a) a statistically significant increase in tritium nuclei content;
(b) a statistically significant number of scintillations from D–D neutrons at 2.45 MeV;
(c) an approximately equal number of D–D MeV neutrons and T nuclei produced;
(d) the generation of D–D neutrons coincident with SL flashes during bubble cloud implosions.

It should be stressed that these effects occurred only in chilled, cavitated D-acetone. The use of D-acetone in the absence of any one of the parameters, for example, PNG or Pu–Be neutron irradiation, without cavitation or in the absence of liquid pool cooling, did not result in nuclear emissions. Moreover, the use of H-acetone never resulted in any statistically significant nuclear emissions.

8 PRODUCTION OF TRITIUM

To detect the tritium (T) content in the liquid used in the present experiment, the tritium decay in a liquid sample taken from the test chamber was measured. This was performed with a Beckman LS 6500 scintillation counter, calibrated to detect the 5–18 keV beta ray decay from tritium.

Before and after the experiments, a 1 cm^3 liquid sample was withdrawn from the upper region of the test section and mixed with an Ecolite scintillation cocktail. The total T content was estimated in the sample by measuring the tritium decay rate. On the assumption that the T concentration was uniform, the total T content in the test chamber was estimated. By subtracting the T content before the experiment (i.e. the background) from that after the experiment, the T production in H-acetone and D-acetone at different liquid pool temperatures (i.e. 0 and 22 °C) was determined, both with and without cavitation and irradiation with the PNG or Pu–Be neutrons. All other experimental conditions were identical, including placing the chamber under standard vacuum conditions. In this way, a series of well-controlled experiments was conducted, changing only one parameter at a time. The chamber was initially filled with H-acetone at 0 °C liquid pool temperature and was irradiated with PNG neutrons for 7 h without cavitation, whereupon any change in T activity was measured. Thereafter, H-acetone experiments with both PNG neutron irradiation and cavitation were performed for 7 h, and, again, any change in T activity was measured. The same process was repeated for 12 h. After verification the absence of T production in the control tests with H-acetone, the experiments with D-acetone were repeated in the same manner with irradiation but without cavitation, and again no statistically significant increase in tritium activity was found (i.e. only $\sim$2 dpm which was well within one standard deviation). In contrast, when D-acetone was cavitated at 0 °C liquid pool temperature, statistically significant tritium production was detected. However, this did not occur when the pool temperature was at 22 °C.

The PNG irradiation and cavitation experiments of 7 and 12 h duration with H-acetone and D-acetone were repeated several times to assure repeatability. A separate test was also conducted over 5 h using a Pu–Be source producing neutrons with constant intensity, constant energy spectrum and in an uninterrupted fashion (i.e. not pulsed as in the case with the PNG). Tritium production was only found for the case of chilled (0 °C), irradiated and cavitated D-acetone.

The results of these experiments are summarized in Fig. 5, which also includes the values of standard deviation (SD). The background (i.e. initial) values of T radioactivity because of detector resolution and some T constituent in the acetone were characterized by a scintillation frequency equal to 17 ± 1.3 dpm, and 53.3 ± 2.3 dpm in D-acetone (where, because of the deuteration process, the background T concentration is higher than in H-acetone). These measurements revealed no significant change in T activity for H-acetone under PNG neutron irradiation, with or without cavitation. Similarly, for the same experimental conditions, irradiation of D-acetone samples with 14.1 MeV neutrons from the PNG, or with neutrons from a Pu–Be source, without cavitation, did not result in any statistically significant change in T content. It should be stressed that no measurable tritium was produced when uncavitated D-

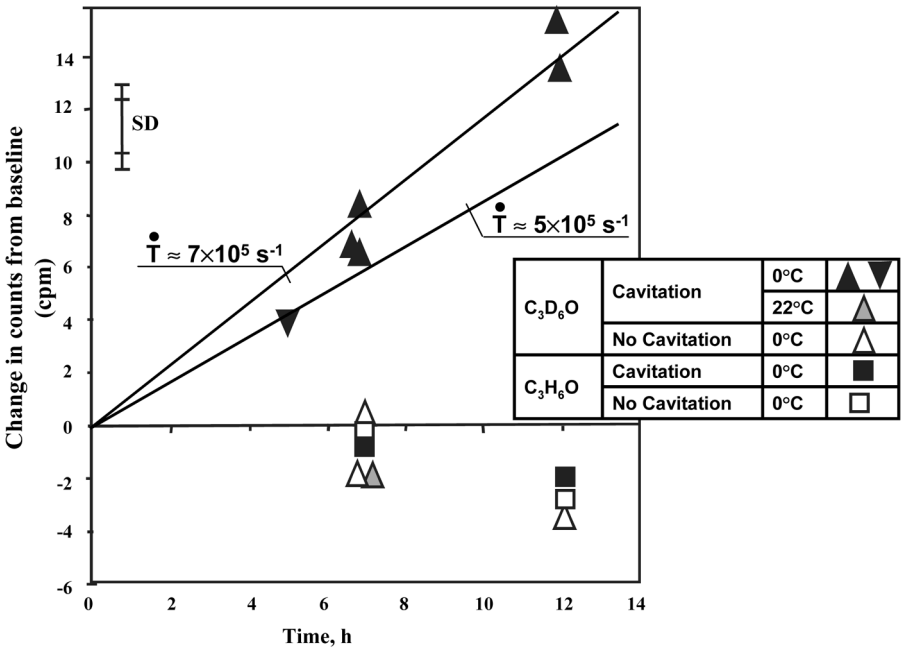

Fig. 5 Changes in the tritium content (i.e. tritium activity) in C_3D_6O and C_3H_6O after neutron irradiation (with PNG or Pu–Be) with cavitation (PZT on) and without cavitation (PZT off), for temperatures of 0 and 22 °C (for C_3D_6O and C_3H_6O the standard deviation was 3.5 and 2.0 counts/min respectively)

acetone was irradiated with fast neutrons. In contrast, in the experiments with cavitated D-acetone at $T_0 \approx 0$ °C and pulsed (from the PNG) or uninterrupted (Pu–Be) neutron irradiation, a statistically significant increase in T activity resulted. In particular, the 5, 7 and 12 h experiments revealed T production, which was directly proportional to the duration of the tests. The T content at these times increased by ~1SD, 2.5SD and 4.5SD above background respectively [**1**]. Finally, as noted previously, the same experiment with D-acetone with cavitation and irradiation from the PNG, over 7 h, but at ~22 °C liquid pool temperature, did not reveal any significant change in T activity. As will be discussed subsequently, this paradox agrees with the results of hydrodynamic shock code simulations of the process. Indeed, these calculations showed a lower speed of the surrounding liquid towards the centre of the imploding bubble, and thus less compression, because of a slower condensation rate at higher pool temperature.

The experiments with a Pu–Be source of neutrons showed (see the experimental point in Fig. 5 corresponding to 5 h) that the continuous production of neutrons was not as effective as for pulsed neutron production. This is presumably due to the fact that the neutrons produced were distributed in time, and thus the bubble clusters were not always nucleated at or near the minimum acoustic pressure, hence the D–D neutron production rate and T production rate were reduced.

If it is assumed that none of the resultant T atoms reacted with D atoms, an inverse calculation based on the observed T activity showed that the intensity of T nuclei and neutron generation due to D–D fusion was reported as $\sim 7 \times 10^5$ n/s [**1**]. Subsequently, more thorough and precise estimates and measurements [**2**] reduced this value to

$$Q_T \sim 3\text{–}5 \times 10^5 \text{ n/s} \tag{3}$$

9 NUMBER OF NEUTRONS GENERATED AND THEIR ENERGY

The neutron intensity was detected by counting the scintillations on the LS or PS. Counts for each mode were recorded over time intervals of 100–300 s. In this case neutron output varied within ± 0.2 per cent under given conditions (i.e. D-acetone or H-acetone, with or without cavitation, and at liquid pool temperature, T_0).

The scintillations were counted in various energy ranges. The first range covered the energy range of scintillations between the lowest detectable value to 2.5 MeV. The second was from 2.5 MeV up to 14 MeV. Subtracting the number of scintillations without cavitation from the number of scintillations with cavitation yielded the increases in the neutron counts, ΔN_1 and ΔN_2, in the two energy ranges.

As shown in Fig. 6, for chilled D-acetone ($T_0 \approx 0$ °C), but not for H-acetone, or for room temperature (22 °C) D-acetone, cavitation results in an increase in $\leqslant 2.5$ MeV neutron scintillations of about 3.7 per cent above background in this energy range for an accumulation of 20 000 sweeps of data of 5 μs duration (i.e. for 100 s). In contrast, in the energy range above 2.5 MeV, no statistically significant increase in scintillations was found.

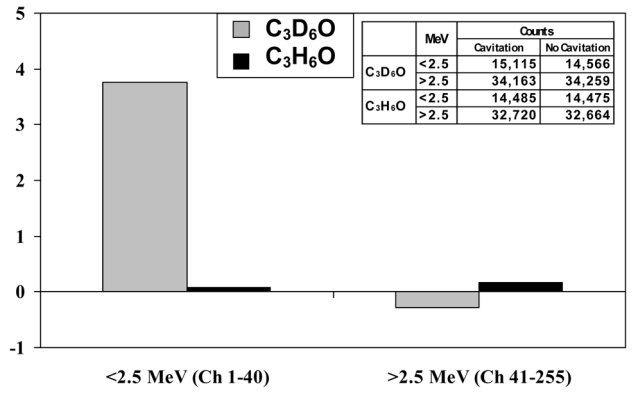

	MeV	Counts	
		Cavitation	No Cavitation
C_3D_6O	<2.5	15,115	14,566
	>2.5	34,163	34,259
C_3H_6O	<2.5	14,485	14,475
	>2.5	32,720	32,664

Fig. 6 Changes in counts for C_3D_6O and C_3H_6O corresponding to energies $E > 2.5$ MeV and $E < 2.5$ MeV for neutron irradiation (PNG on) with cavitation (PZT on) and without cavitation (PZT off). The data acquisition times were 100 s (<2.5 MeV) and 300 s (>2.5 MeV)

These experiments were repeated many times, and hence the change in the number of scintillations by (3.7 ± 0.4) per cent represents a statistically significant increase of about 10SD above background [**1**]. In subsequent experiments [**2**] the statistical accuracy was increased to about 60SD. The observed increase in scintillations corresponds to the detection of 5–6 neutrons per second. Considering that the estimation given in equation (2) for the efficiency of the detector for neutrons emitted from the acetone-filled flask is equal to $(0.5–1) \times 10^{-4}$, the measured intensity of neutron production was

$$Q_n = \frac{5–6}{0.5–1 \times 10^{-4}} = (0.5–1.2) \times 10^5 \text{ n/s} \quad (4)$$

Subsequent measurements using a more efficient detection system [**2**] have given a higher production rate of D–D neutrons, $\sim 4 \times 10^5$ n/s. This value is fully consistent with the neutron generation inferred from the measurements of T production, $\sim(3–5) \times 10^5$ n/s, and thus the tritium measurements are fully consistent with the measurements of D–D neutrons.

10 COINCIDENCE BETWEEN NEUTRON AND SL SIGNALS

The coincidence between the SL (i.e. the PMT) and the PS/LS neutron pulses was also examined. Three modes were tested for data acquisition and the number of coincidences between the photomultiplier tube (PMT) and PS/LS signals. In mode 1, records of such coincident signals were obtained by direct analysis of the oscillograms on a digital storage oscilloscope triggered by the SL signal, at a low bias voltage for the PMT (-300 V), which resulted in the elimination of false signals but reduced PMT sensitivity (the frequency of luminescent signals in the PMT was $\sim$0.1/s using a bias voltage of -300 V, and these were SL flashes during bubble implosion; under a bias voltage of -450 V the frequency of luminescent signals was 1–5/s, among which about 30 per cent were false signals, being induced by so-called 'dark current' [**28**] and/or PNG neutrons). In this mode no SL signals occurred in the PMT during PNG operation (i.e. neutron-induced false SL activity was excluded), but many of the genuine SL signals due to bubble implosions were also rejected. In this mode, coincidence between SL signals in the PMT and scintillations in the PS/LS repeatedly took place for cavitated D-acetone at $T_0 \approx 0$ °C. Figure 7 gives a typical data trace for tests with chilled, cavitated D-acetone [**1**], showing coincidence between the SL flash and the neutron pulse. Also, the subsequent acoustic (shock) signal on the flask wall, as noted in the discussion of Fig. 2, can be seen. No such coincidences were seen for tests with H-acetone. However, data acquisition in mode 1 operation (using a 100 MHz four-channel digital storage oscilloscope) was slow, and many genuine SL signals were not recorded at such a reduced PMT sensitivity.

In the second mode of operation, only double coincidences (SL signal in the PMT, and PS or LS pulse), with ± 2 μs accuracy, were considered. The bias voltage to the PMT was -450 V, which resulted in higher sensitivity. As a consequence, the PMT recorded weaker light signals as well, among them not only the SL flashes from bubble implosions but also light flashes induced by neutrons or gamma ray emissions. Each signal in the PMT triggered scintillation counting in the PS or LS which was binned in $\Delta t = 2$ μs bins from $t_L - 3\Delta t$ to $t_L + 3\Delta t$, where t_L is the moment of the noted luminescence (in particular, sonoluminescence) signal in the PMT. The number of scintillations in each of these six time intervals was counted twice, with and without cavitation. Luminescence signals induced by neutrons or gamma rays in the PMT could be random, almost simultaneous or close in time (± 2 μs) with the neutron scintillations in the PS or LS and gave a number of false coincidences. The number and intensity of such false, or background, coincidences were determined by the number of scintillations in the above-mentioned intervals relative to the detected luminescence signals in the PMT under PNG operation, but without cavitation (i.e. without PZT operation), leaving all other parameters the same. The genuine number of coincidences (GNC) with cavitation was found by subtracting the number of false, or background, scintillations taken in each interval, without cavitation, from the corresponding total number of scintillations taken with cavitation.

Figure 8 gives the distribution of the number of such scintillations within the time intervals in relation to luminescence signals in the PMT for D-acetone and H-acetone, with and without cavitation. Figure 9 gives the GNC above background for D-acetone and H-acetone at different temperatures (including the conditions shown in Fig. 8).

It can be seen that only for tests with chilled (i.e. $T_0 \approx 0$ °C) cavitated D-acetone, and only within the time interval $t_L \pm 2$ μs, was there a sharp GNC peak. Outside

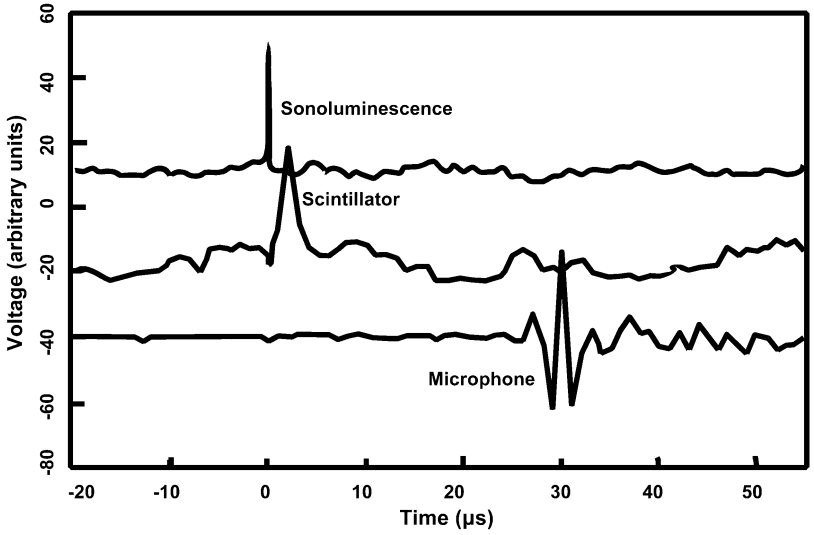

Fig. 7 Representative time variation in PMT (SL) flashes, the scintillator nuclear signal and microphone shock wave trace signals (C_3D_6O, cavitation experiments at 0 °C)

this interval (and especially beyond ± 4 μs) the GNC was within 1SD and thus not statistically significant. No such GNC peaking was seen for H-acetone. Similar data for D-acetone were obtained at $T_0 \approx 19$ °C and $T_0 \approx 21$ °C, and at these temperatures no significant GNC were seen. As in the case of the previously discussed measurements for tritium production, this shows that no neutron production took place in room temperature D-acetone, although, as expected, there were SL emissions due to bubble implosion.

The time required to obtain 100 coincidences was about 30 min on average. The standard deviation was calculated by extracting the square root of the sum of counts in each time interval (2 μs) during bubble implosion and SL light emission. Using MCA time spectrum data, the instantaneous scintillation frequency from neutrons and gamma rays during bubble implosion and SL light emission was calculated, and it was about 1–50/s. For a time window of 20 μs, the frequency of SL signals was about 1 flash per second, and the counting period of coincidences was

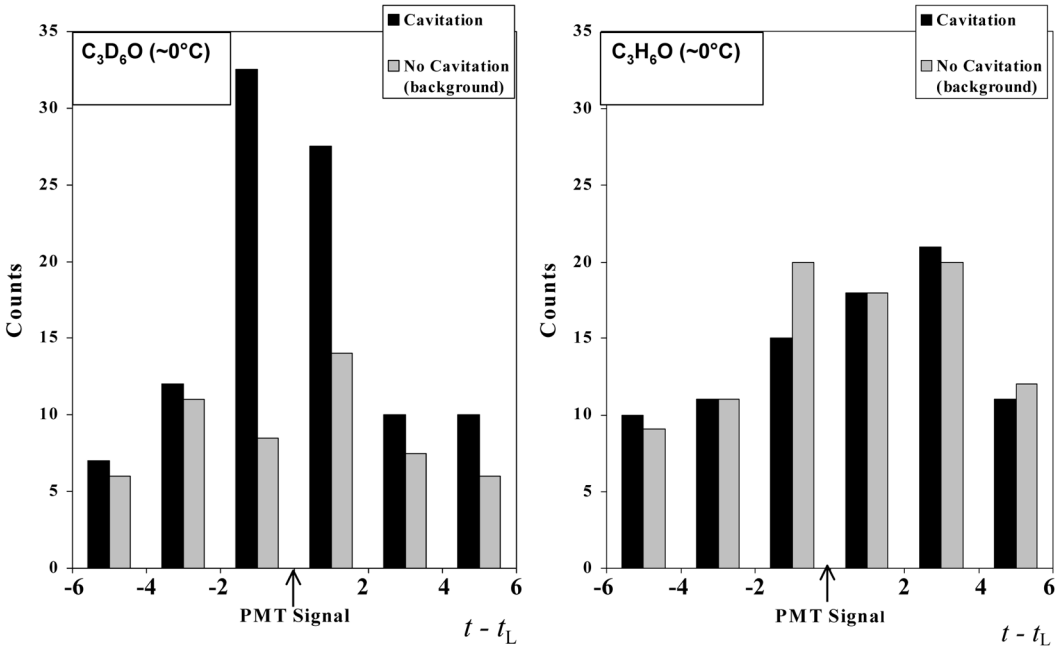

Fig. 8 Distribution of the number of neutron scintillations (in PS/LS) in relation to luminescence signals in the PMT (regime 2) for chilled C_3D_6O and C_3H_6O

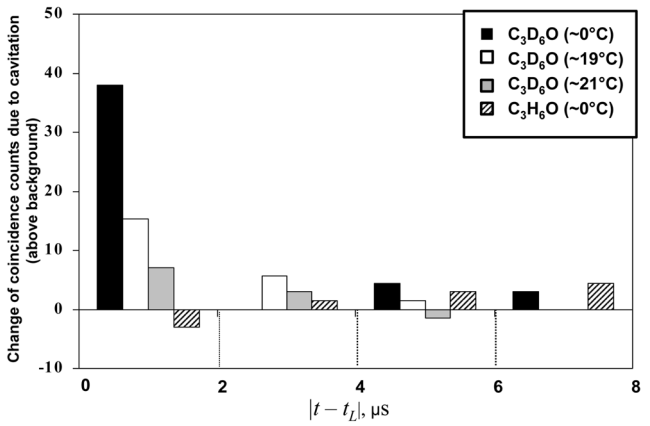

Fig. 9 Distribution of the coincidence counts (regime 2) in C_3D_6O and C_3H_6O versus $|t - t_L|$.

$\sim$1800 s. The number of random coincidences was estimated to be negligibly small: $(20 \times 10^{-6}\ \text{s}) \times (1-50/\text{s}) \times 1/\text{s} \times 1800\ \text{s} \sim 0.036-1.8$.

In mode 2 operation, data were obtained in a two-channel 500 MHz oscilloscope. Simultaneous time spectra data were not possible for the SL and scintillator signals, but these were measured separately under identical experimental conditions. These series of experiments revealed insignificant deviations in nuclear and SL signal counts. The data were then used to estimate random coincidences. It was found that coincidences occurring during the time of PNG operation were random. However, as discussed above, the random coincidences during bubble implosions were insignificant.

The natural question arises as to the reason for higher GNC within the interval of -2 μs to 0 μs, that is, before the SL signal. The reason is that SL flashes in the PMT should occur in groups mainly over 5 μs (i.e. when a SL signal was recorded in the PMT), and as a rule they were preceded by several SL signals from neighbouring bubbles in the imploding bubble cluster, which were unrecorded by the PMT. Another question is the reason for there being a GNC for 2 μs after a SL signal. It takes about 0.04 μs for a 2.45 MeV neutron with a speed of $\sim 2 \times 10^6$ m/s to reach the scintillator in a straight path (about 7–8 cm from a cavitation bubble). Apart from the fact that a neutron might be emitted later than a recorded SL flash, because of an unrecorded SL flash from a neighbouring bubble (which may collapse within ± 3 μs), some of the neutrons from a collapsing bubble can collide with the liquid nuclei and other elements of the experimental system, thus losing energy and extending their path before they hit the PS/LS. Therefore, these neutrons may arrive at the scintillator later than the time of their generation (i.e. -0.04 μs).

In mode 3 operation, a multichannel analyser was used to measure and record the time history of the number of nuclear scintillations (due to neutrons and gamma rays) during the first 100 μs after initiation of a PNG pulse (at $t = 0.0$ μs). Figure 10 shows that, for the case of chilled, cavitated D-acetone, an increase in the number of these scintillations falls in the time interval from $t_{1C} = 27 \pm 3$ μs to $t \approx 42$ μs (channels 96 to 130) where the SL signals appear to be intense during bubble implosion (see Fig. 3). No increase was seen with H-acetone and room temperature D-acetone. This increase is statistically significant (about 5SD). In this case the background (without cavitation) values of the number of scintillations that are found in channels 70 to 255, and correspond to the time after the completion of a PNG neutron pulse, were 198 ± 3.

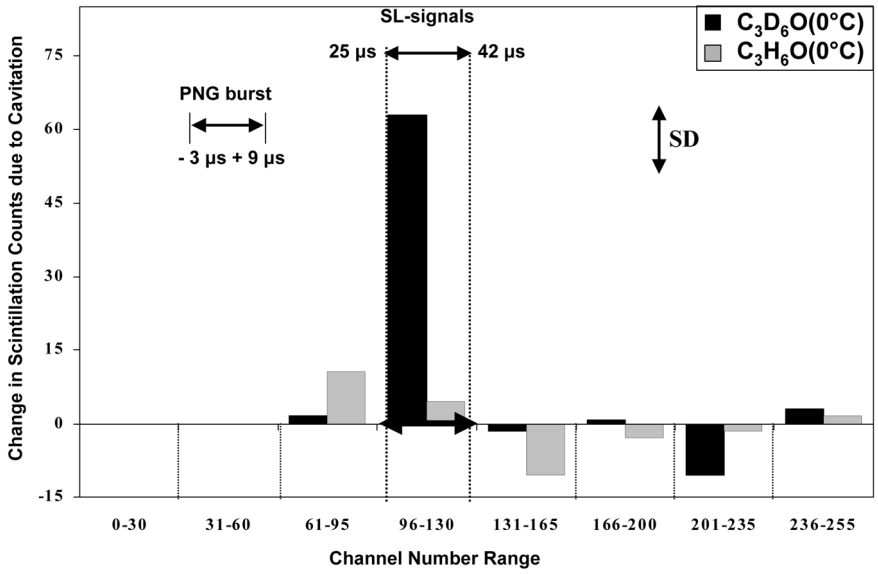

Fig. 10 Distribution of the increase in nuclear scintillations (due to neutrons and gamma rays in PS/LS, regime 3) because of the cavitation (PZT on) during the first 100 μs after initiation of a PNG

Finally, as noted previously, the insets in Fig. 4 also show strong coincidence between D–D neutron emissions and SL light pulses during the time interval in which the bubble cluster implosions were being driven acoustically [**2**].

11 ANALYSIS OF SOME INDEPENDENT MEASUREMENTS AT ORNL

Prior to the publication of the initial paper of the present authors in *Science* [**1**] some members of the Physics Division (PD) at Oak Ridge National Laboratory, D. Shapira and M. Saltmarsh, performed independent neutron measurements, using the same experimental apparatus as that described in section 3 but another neutron detector (hereafter called the PD detector) of volume $V_{PD} = 3000\ cm^3$, which was 30 times larger than the Elscint (i.e. ET) liquid scintillator ($V_{ET} = 100\ cm^3$) that was used in the present measurements. Shapira and Saltmarsh criticized the present author's measurements [**36**] and claimed that the neutron production rate, Q_n, they measured was at least several orders of magnitude less than that stated in the *Science* paper [**1**]. A Web supplement [**37**] gives a detailed analysis of the PD system for measuring neutrons in the present experiment and the problems they had measuring coincidence between SL and neutron signals.

Figure 11 gives a schematic representation of the measurement systems using the ET and PD detectors. Because of its considerable size, the PD detector could not be placed inside the refrigerated test section, which maintained the required low temperature (0 °C) in the flask filled with liquid D-acetone. As a result, the massive and more sensitive PD scintillator had a solid angle ($\varphi_{PD} \sim 0.012$ rad) that was almost 6 times less than the solid angle of the ET detector ($\varphi_{ET} \sim 0.07$ rad). The efficiency of the PD detector in the configuration shown in Fig. 11, as well as that of the ET detector [see equation (2)], was determined using a Pu–Be neutron source of known intensity (2×10^6 n/s). When this source was placed at a distance of 30 cm from the PD, the efficiency for detection of neutrons was $\sim 2 \times 10^{-4}$; for 2.45 MeV neutrons this corresponds to an efficiency of $\sim 10^{-4}$. As discussed in section 3, about 50 per cent of the 2.45 MeV D–D neutrons were attenuated in the test section and liquid acetone-filled flask, while about 50 per cent of the neutrons penetrating the flask were dispersed and lost a great deal of energy in the refrigerating chamber walls. Also taking into account that the actual distance from the zone of cavitation was about 42 cm, the efficiency of the PD detector for detecting 2.45 MeV neutrons in the discussed configuration was

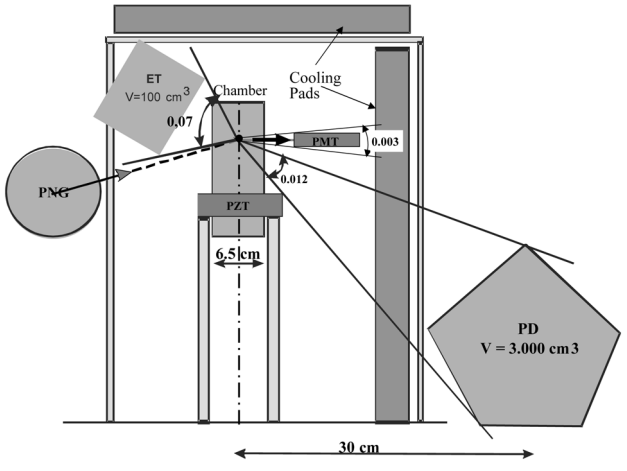

Fig. 11 Comparison of detection systems for D–D neutrons using ET [**1**] and PD detectors [**36**]

$$\eta_{PD} \sim 10^{-4} \times 0.5 \times 0.5\left(\frac{30}{42}\right)^2 \sim 10^{-5} \quad (5)$$

which, as can be seen in equation (2), is about 10–20 times less than in the case of the ET detector.

Nevertheless, in the measurements made by Shapira and Saltmarsh, signals were observed of neutron scintillations corresponding to energies less than or equal to 2.45 MeV. The measured increase in neutron counts above background was equal to ~3 n/s. Taking into account the efficiency of the ET detector gives an intensity of neutron production $Q_n \sim 3 \times 10^5$ n/s, which is quite similiar to that measured with the ET detector. Thus, the conclusions on fusion neutron production given by Shapira and Saltmarsh [**36**] appear to be a consequence of a gross overestimation of the measurement efficiency of their detector.

Furthermore, Shapira and Saltmarsh reported that they found no time coincidence between the neutron and SL signals. Again, this was a consequence of their measurement system being inappropriately chosen. In the measurement system of the present authors a luminescence signal (corresponding to a SL signal) triggered the counting of either neutron signals alone (mode 2 with PSD) or any nuclear scintillations (mode 3), among which the contribution of neutron scintillations was about 50 per cent owing to the relatively small volume of the ET scintillator. As a result, an increase in scintillations over a narrow time interval (± 2 μs) close to the SL signals was found. In contrast to the present experimental technique, Shapira and Saltmarsh [**36**] used the nuclear scintillation signal to trigger the counting of luminescence signals. The PD detector could not perform PSD owing to gamma ray saturation effects (i.e. the gamma/neutron ratio in their detector was at least 30 to 1). As a consequence, the contribution of neutron scintillations was less than 3.0 per cent because of the relatively large volume, V_{PD}, of their detector. Therefore, the great bulk of the scintillations (triggers), after which an increase in SL signals during cavitation were looked for (over a narrow time interval of ± 2 μs), were not due to neutrons. This means that coincidences between scintillations and luminescence signals were essentially (~97 per cent) random in nature. Thus, the system employed by Shapira and Saltmarsh to measure time coincidences between

neutron and SL signals was not appropriate for this purpose. Nevertheless, Shapira and Saltmarsh [**36**] measured a very interesting build-up of nuclear emissions at the acoustic frequency beginning about ten acoustic cycles after the initial energetic bubble implosion. It was not possible to see this phenomenon in the experiments reported in *Science* [**1**], since the measurement system used would not allow data acquisition for a long enough time interval. Subsequently, a new measurement system detected the same phenomenon [**2**], which is apparently due to the shock wave in the liquid associated with the initial implosion interacting with the vibrating wall of the acoustic chamber, thus detuning the acoustic standing wave for about ten acoustic periods. These new data are given in Fig. 4, and they show that most of the D–D neutrons are actually produced after the violent initial implosion, where the bubble cloud is imploding (i.e. bouncing) at the acoustic frequency. Note the build-up of D–D neutron counts by $\sim$1 ms after the PNG fires and the decay (presumably as a result of condensation and/or expulsion of the vapour bubble cloud from the acoustic antinode owing to the Bjerknes force [**23**]) of the nuclear emissions from the vapour bubble cloud by $\sim$2.5 ms.

Finally, Lillie *et al.* [**38**] performed neutronic simulations in an attempt to assess the data of Shapira and Saltmarsh [**36**]. However, they assumed a PNG pulsed neutron production rate that was about twice that in the present authors' experiments, and they took no account of saturation of the PD detector, thus their conclusions are not reliable. Nevertheless, they do show that a rate of neutron-induced gamma ray emissions that is about 10 per cent of that for the emitted 2.45 MeV D–D fusion neutrons should be expected. Interestingly, the most recent bubble fusion experiments at ORNL have confirmed the validity of this result [**2**].

12 THEORETICAL ANALYSIS OF BUBBLE IMPLOSION

To obtain an estimate of the implosive collapse conditions and the possibility of D–D nuclear fusion in the experiments described above, a transient one-dimensional hydrodynamic shock code (i.e. a HYDRO code) was developed which accounted for the heat, momentum and mass exchange processes in and around a vapour bubble. This model includes the partial differential equations for mass, momentum and energy conservation and the interface conditions accounting for non-equilibrium phase change (i.e. evaporation and condensation). The phase change process was evaluated using a Hertz–Knudsen–Langmuir kinetic model which uses an accomodation coefficient, α. Use was also made of Mie–Gruniesen equations of state [**39**] which account for the intermolecular or interatomic interactions in the form of a Born–Mayer potential function and its extensions [**40**]. These equations of state are known to be valid for highly compressed fluids. Parameters for the equation of state for acetone were calculated on the basis of available thermodynamic data (in particular, in the two-phase region[†]) and the experimental shock wave adiabatic data for liquid acetone measured by Trunin *et al.* [**41**]. Account was taken of the dynamic effects of dissociation and ionization, and of the strong temperature dependence on thermal conductivity [**39**] during plasma formation within the imploding bubbles. Account was also taken of the state of thermal non-equilibrium among the ions and electrons formed during the 10^{-13}–10^{-12} s time interval associated with the final stage of the bubble implosion process. Figure 12 implicitly gives the equation of state that was used. Note the non-linear dependence of the acetone isotherms, including the zero isotherm (corresponding to $T = 0$ K). The Grüneisen coefficients, Γ, for various degrees of acetone dissociation (Dis) and non-dissociation (NDis) are also shown. These curves give the equation of state for D-acetone for densities ranging from 10^{-3} to 50 g/cm^3 and temperatures ranging from 250 to 10^8 K.

The temperature dependence of vapour thermal conductivity, including the plasma state, has the form

$$\lambda = \lambda_0 \left[1 - k_0' + k_0' \left(\frac{T}{T_0} \right)^{\theta} \right], \quad \lambda_0 = 8.23 \times 10^{-3} \text{ kg m/(s}^3 \text{ K)}, \quad k_0' = 75, \quad \theta = 0.5 \tag{6}$$

where λ_0 is the well-known molecular thermal conductivity for the initial conditions ($T/T_0 = 1.0$). The asymptote (i.e. $T/T_0 \gg 1.0$) of this model, $\lambda = \lambda_0 k_0' (T/T_0)^{\theta}$, was derived using the theory of Zeldovich and Raizer [**39**] for the thermal conductivity of ions. Parametric HYDRO code runs were made to assess the sensitivity of the results to equation (6), and, as will be discussed below, it was found that the influence was not significant.

Using all these equations, a HYDRO code based on Godunov's numerical integration technique was developed [**42**]. Bubble dynamics was examined for conditions similar to those in the present bubble fusion experiments (more details on this model and its results are available at *www.rpi.edu/* $\sim$ *laheyr/DARPA_Slides_Nigmatulin-Lahey.ppt*).

It is very important to remember that bubble growth and almost all of the compression process ($\sim$25 μs in duration at 19.3 kHz) occur with values of radial interface velocity, $|\dot{R}|$, less than $\sim$50 m/s. Under these conditions of a small gas/vapour Mach number ($M_g \equiv |\dot{R}|/C_g$), the gas/vapour pressure in the bubble is uniform and does not exceed 10 bar. This process may be described by a reduced set of equations

[†]Moss *et al.* [**20**] recognized that they did not know how to account for phase change with vapour (in their case it was water vapour added to deuterium), and the equations of state related to the two-phase region. Thus, they considered the vapour as air. In the present investigation, phase transformations of the vapour/liquid type were taken into account explicitly, and this phase transformation was crucial during the implosion process.

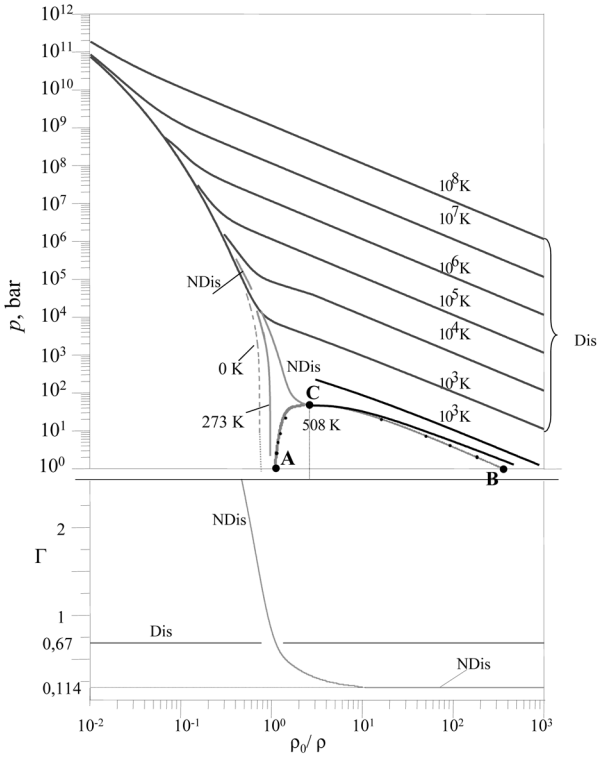

Fig. 12 Isotherms, Grüneisen function, Γ (for vapour, $\Gamma = \gamma - 1$, where γ is the ratio of specific heats), and the critical region for acetone ($\rho_0 = 0.858$ kg/m^3 at atmosphere conditions): dashed line = zero isotherm (corresponds to non-dissociated acetone at $T = 0$ K); C = critical point; ACB = boundary of two-phase region; Ndis and Dis indicate non-dissociated and dissociated matter respectively

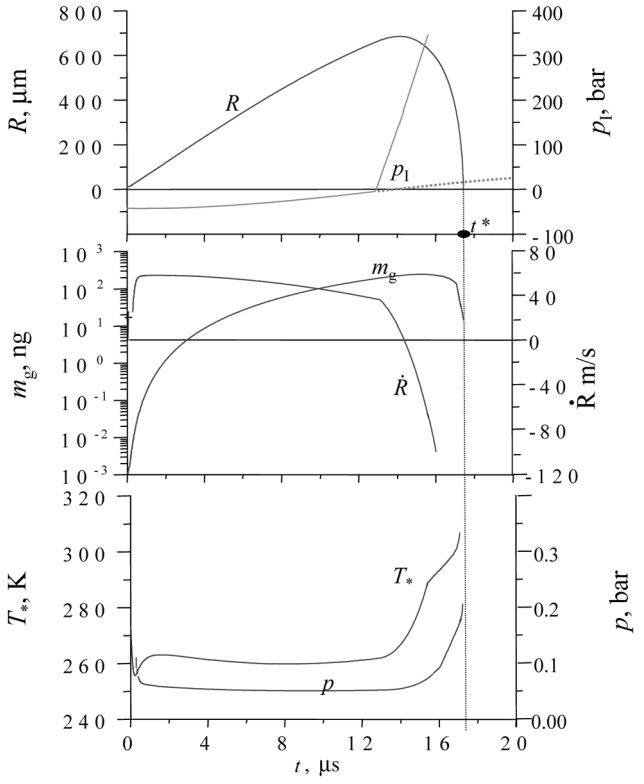

Fig. 13 Time evolution of the vapour bubble radius, R, interface velocity ($w = \mathrm{d}R/\mathrm{d}t \equiv \dot{R}$, approximately equal to the radial liquid velocity at the interface), vapour mass, m_g, vapour pressure, p, and temperature T_*, in the bubble during subsonic conditions. Results are presented for an acoustic pressure amplitude of $\Delta p_I = 40$ bar, an acoustic frequency of $f = 20$ kHz and a liquid pool temperature $T_0 = 0\ ^\circ$C. The actual liquid pressure amplitude within the bubble cluster during implosions may be intensified by at least several hundred bar owing to bubble cluster dynamics

that includes an extended Rayleigh–Plesset equation for bubble radius and the equations for heat and mass exchange in the vapour and liquid. Moreover, in this case the gas (of low density) behaves in accordance with the perfect gas law. Typical computational results for this relatively slow (i.e. low gas Mach number) stage are shown in Fig. 13. During the expansion stage of bubble dynamics, an accumulation of potential liquid kinetic energy takes place. During the implosion stage, some of this energy will be transformed into internal energy in the liquid around, and the vapour/plasma inside, an imploding bubble. It is important to note that 50–90 per cent of the vapour created by evaporation at the time of maximum bubble size is condensed during the bubble implosion phase.

Close to the final stage of bubble collapse, during a nanosecond time span, compressibility effects are important even in the liquid (i.e. the liquid density increases by a factor of 2 or 3 near the interface), as are shock waves, gas/vapour densities, pressures and vapour temperatures near the bubble centre. The vapour transforms into a state of dissociated and ionized high-density plasma. During this phase of bubble implosion, the imploding vapour bubbles reach a minimum radius of about $R_{\min} \approx 10\ \mu$m, and the radial velocity of the liquid moving towards the bubble centre is $(w_L)_{\max} \sim 7$ km/s at the interface.

A picosecond time range follows next, where the liquid at the interface is accelerated to enormous speeds, initiating shocks and/or quasi-shock compression waves in the vapour, which converge and focus towards the bubble centre. As the shock wave is focused, the plasma temperature and pressure reach very high levels as the wave arrives at the centre. Thereafter, the shock wave, which is reflected from the centre, diverges and becomes weaker with radial distance. Nevertheless, the bubble continues to implode for a brief interval, and this further compression leads to an additional increase in temperature and vapour density. The closer to the centre, the higher are the temperature, vapour/plasma density and potential for thermonuclear reaction rate, but the shorter are the duration of this state and the

reaction time, and the amount of material to react is also much less. This sequence is shown in Fig. 14 at five different times using two different assumptions for thermal conductivity [i.e. constant thermal conductivity and equation (6)]. Significantly, the final results are insensitive to the model used for thermal conductivity.

To estimate the neutron and T production rate per unit volume as a result of D–D nuclear fusion, use was made of a kinetic equation for the fusion rate due to D–D nuclei collisions [**43**]

$$J_n = \tfrac{1}{2} n_{\mathrm{D}}^2 \langle \sigma\, v \rangle \approx J_{\mathrm{T}} \tag{7}$$

where n_{D} is the D nucleus concentration and $\langle \sigma\, v \rangle$ is the reactivity, which is equal to the averaged product of the cross-section, σ, and the D nucleus speed, v [**44**]. The reactivity is determined by the ion temperature, T_{i}. At $T_{\mathrm{i}} = 10^8$ K, the reactivity, $\langle \sigma v \rangle$, is 3×10^{-25} m^3/s. For D-acetone (C_3D_6O) n_{D} is determined by

$$n_{\mathrm{D}} = \frac{6\rho_{\mathrm{g}} N_{\mathrm{A}}}{M_{\mathrm{g}}} = \rho_{\mathrm{g}} N_{\mathrm{m}} \qquad \left(N_{\mathrm{m}} = \frac{6N_{\mathrm{A}}}{M} = 0.565 \times 10^{26}/\mathrm{kg} \right) \tag{8}$$

where N_{A} is the Avogadro number and M is the molecular weight ($M = 64$ kg/kmol for D-acetone with six deuterium nuclei in each molecule).

The total neutron and tritium production per implosion is defined by the integral taken over the bubble volume, V_{b}, and the time from the expression for fusion rate density, J

$$Q = \int_{V_b} \int_{1/f} J \, \mathrm{d}V \mathrm{d}t = \int_0^R q(r) \, \mathrm{d}r, \qquad \text{where } q(r) = 4\pi r^2 \int_0^{1/f} J(r,t) \, \mathrm{d}t \tag{9}$$

where $q(r)$ characterizes the D–D fusion rate at each radial position. The HYDRO code predictions for different values of thermal conductivity show that neutron and T production has a peak at $r_* \approx 10$ nm and the total production takes place within a radius $r_{\mathrm{c}} \approx 50$–$80$ nm (see Fig. 15). In spite of the fact that the maximum temperatures and densities are higher at $r < r_*$ than at r_*, these ultrahigh conditions at smaller radii exist only for a very short time and occupy a very small volume (having very little mass).

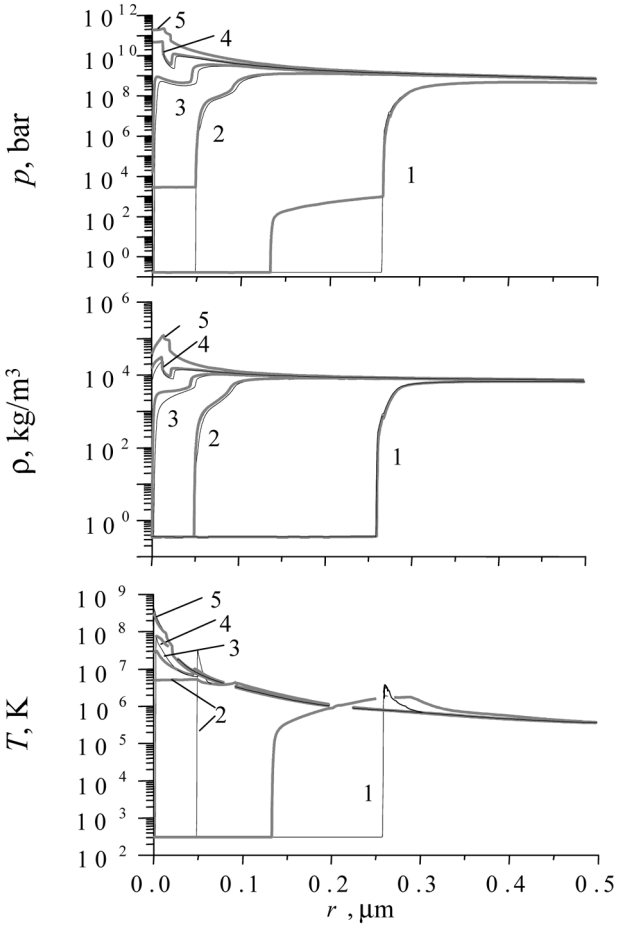

Fig. 14 Focusing of the shock wave at the bubble centre (picosecond stage). Thin lines are the solution with constant heat conductivity ($k = k_0$), thick lines are the solution with heat conductivity that satisfies equation (6). Numbers indicate parameter distributions at times $t_1 = 0.0$, $t_2 = 0.61$, $t_3 = 0.68$, $t_4 = 0.72$ and $t_5 = 0.76$ ps, with respect to an arbitrary starting time

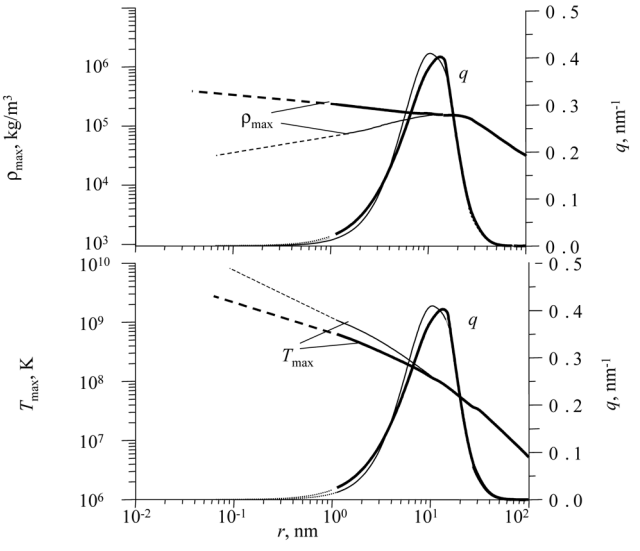

Fig. 15 Neutron production per unit radial length, q, maximum plasma temperature, $T_{\max}$, and maximum plasma density, $\rho_{\max}$, as functions of the radial coordinate. Thin and thick lines are the same as in Fig. 14, and the dot and dash lines indicate different levels of spatial nodalization

This is why there is a maximum value of the function $q(r)$ at a finite radius. In the present calculations, the characteristic values for parameters at radius r_*, namely the time interval Δt_*, density ρ_*, pressure p_*, ionic temperature, T_{i^*} and interfacial velocity w_*, were {note that the pressures, temperatures and interface velocity are several orders of magnitude larger than for typical SBSL experiments [see equation (1)]}

$$r_* \sim 10\text{–}20\,\text{nm}, \quad \Delta t_* \sim 10^{-13}\,\text{s}, \quad \rho_* \sim 10\text{–}100\,\text{g/cm}^3,$$
$$p_* \sim 10^{11}\,\text{bar}, \quad T_* \sim 10^8\,\text{K}, \quad w_* \sim 900\,\text{km/s} \qquad (10)$$

With a slight decrease (as compared with these temperatures) in liquid pool temperature from room temperature ($T_0 \approx 20\,^\circ\text{C}$) to $T_0 = 0\,^\circ\text{C}$ and below, the neutron and T production grows significantly. This is because, during bubble growth, less vapour is evaporated in a low-temperature liquid, and, more importantly, during bubble implosion, more vapour is condensed. This results in less vapour and higher kinetic energy of the liquid by the time of initiation of a shock wave moving towards the bubble centre through the remaining compressed vapour. As a consequence, for a low-temperature liquid pool, an increase is found in the intensity of the focusing shock wave and the extent to which the plasma in a sphere of radius r_* is compressed and heated. As already discussed in sections 7 and 8, this paradoxical effect of liquid temperature has been experimentally verified. This clearly shows the synergy of the experiments and analysis, and how they aid each other in interpreting bubble fusion phenomena.

Similarly, larger values of the condensation (i.e. accommodation) coefficient, α, yields more condensation and less increase in pressure during the early phase of bubble collapse which is favourable to higher interfacial acceleration and ultimately to more intense vapour compression. Significantly, organic fluids, with their relatively large and bulky molecules, have greater coefficients of condensation, approaching $\alpha \approx 1.0$ [**45**]. Therefore, deuterated organic fluids offer advantages over, for example, heavy water which has a relatively small coefficient, $\alpha \approx 0.075$ [**46**–**48**]. Moreover, it is difficult to expose water (as opposed to organic fluids such as acetone) to large levels of tension without having premature cavitation. Thus, D-acetone (C_3D_6O) was chosen in the present experiments since it appeared to be a much better test fluid for bubble fusion than heavy water (D_2O).

HYDRO code simulations have also shown that, for the case of a single bubble subjected to acoustic forcing with an amplitude of 15 bar, neutron and T production is insignificant. It is important to stress that there are bubble clusters formed by the PNG neutrons, and an increase in the liquid pressure by many factors occurs in the central region of an imploding bubble cluster [**40**]. This was taken into account by applying the predicted increase in the incident pressure acting on the interior bubbles during acoustic compression (e.g. see the solid p_I line for $t \geqslant 13\ \mu$s in Fig. 12).

Another important observation is the absence of 'cold' fluid dissociation at the interface for pressures of the order of 10^5 bar. This makes the fluid more rigid (i.e. less compressible because the structure of the molecules is preserved) compared with the equilibrium dissociated atomic structure. For the liquid, which is relatively 'cold', dissociation of the molecules requires a dissociation time $t_D \sim 10^{-7}$ s. However, HYDRO code simulations indicate that highly compressed conditions on the liquid side of the interface are sustained for only $\sim 10^{-9}$ s. Thus, significant dissociation of the liquid does not have time to take place, and the resultant stiffer non-dissociated liquid creates a stronger shock wave in the vapour, leading to significantly higher peak pressures and temperatures in the interior of the imploding vapour bubbles.

Moreover, in typical MBSL and SBSL experiments with non-condensible gas bubbles, endothermic chemical reactions (associated with the dissociation and ionization processes within the gas/vapour bubble) significantly limits the temperature rise [**49**, **50**]. In bubble fusion experiments there are also endothermic chemical reactions within the imploding bubble, but they do not significantly reduce the peak temperatures and D–D neutron production rates, since the maximum possible reduction in peak temperature owing to endothermic dissociation and ionization processes is less than about 10 per cent; that is, about 10^7 K out of at least 10^8 K [**42**] (see *www.rpi.edu/~laheyr/DARPA_Slides_Nigmatulin-Lahey.ppt* for more details).

It is also important to note that the ionized plasma remains essentially in non-equilibrium, with the electron temperatures being significantly below the ion temperatures (i.e. $T_e \ll T_i$), over the period of the fusion reactions ($\sim 10^{-13}$ s), since the electrons have insufficient time to be appreciably heated by the ions. This reduces the electron-related energy losses significantly (e.g. bremsstrahlung, line and recombination losses, etc.), and it is necessary to evaluate only the ion temperature, T_i (i.e. a two-temperature plasma dynamics model is not needed).

For the experimental conditions reported in the present author's *Science* [**1**] and *Physical Review—E* [**2**] papers, Fig. 16 shows that the HYDRO code predictions indicate a neutron production of about 7 neutrons per implosion per bubble. High-speed photographic evidence of bubble clusters indicated that there were about 1000 bubbles in each bubble cluster in the present experiments. Moreover, about 50 implosions/s were observed (i.e. shock waves associated with the energetic first implosions of the bubble cluster which, as seen in Fig. 7, were picked up on the microphones on the wall of the acoustic chamber). Analysis of the bubble cloud dynamics indicated that about 2 per cent of the interior bubbles in each bubble cluster (i.e. ~20 bubbles) undergo energetic implosions, and Fig. 4 indicates that there are about 60 subsequent implosions (i.e. bounces) of the bubble cluster after each initial implosion. Thus, HYDRO code predictions imply a D–D neutron production rate of about 4×10^5 neutrons/s (i.e. 7 neutrons/bubble bounce × 20 bubbles × 50 implo-

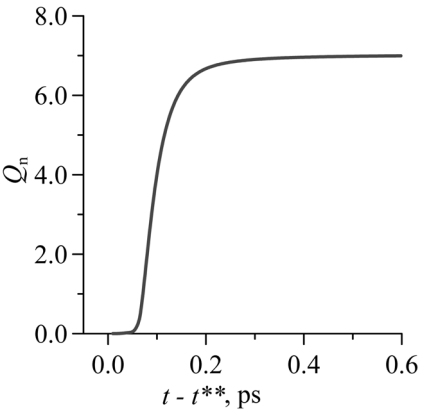

Fig. 16 Predicted cumulative D–D neutron production; that is, Q_n versus time from the onset of neutron production at r^* ($\sim$10 nm), where t^{**} is the time (ps) at which significant neutron production starts

sions/s $\times$ 60 bounces/implosion), which is consistent with measurements of the T and D–D fusion neutron production rates [**1**, **2**]. In any event, the HYDRO code predictions indicate conditions that are suitable for D–D fusion.

In subsequent investigations, more detailed models will likely be developed to improve the plasma physics (e.g. the kinetics of the dissociation and ionization processes), the nuclear physics and the pressure intensification process within a bubble cluster. Nevertheless, the basic conclusions discussed above are expected to remain unchanged.

13 POTENTIAL APPLICATIONS OF BUBBLE FUSION

It is too early to understand the full implications of bubble fusion technology, but it appears to be very promising. For example, it may offer important new ways to study parametrically the plasma physics and neutron cross-sections associated with nuclear fusion processes. Also, if the neutron production rate is properly scaled up (e.g. by optimizing the test liquid, lowering the liquid pool temperature and/or using deuterium–tritium (D–T) reactions, etc.), an interesting new picosecond duration pulsed neutron source could be available for use in a wide range of scientific studies in, for example, solid state physics and material science. Moreover, bubble fusion might be used in novel new production facilities for tritium and/or helium-3. In addition, there are always medical applications for a relatively low-cost neutron source.

However, the 'holy grail' of all fusion research is to find a safe, environmentally friendly way to produce energy for practical applications (e.g. electric energy production). The present situation is analogous to being somewhere between the discovery of nuclear fission by Otto Hahn and Lisa Meitner and the demonstration of a nuclear chain reaction by Enrico Fermi. Indeed, much more research will be needed to determine whether bubble fusion can be scaled up sufficiently to be able to produce commercially interesting amounts of energy. Nevertheless, this exciting new technology appears to be inherently safe (i.e. no significant decay heat will be present after shutdown) and environmentally friendly (i.e. the tritium produced is a fuel to be consumed in D–T reactions, and thus it should be possible to minimize radioactive waste products).

Only time will tell what the practical significance of bubble fusion phenomena may be, but, for sure, it is an interesting and challenging application of multiphase science and nuclear engineering principles.

ACKNOWLEDGEMENTS

Sponsorship of this research by the US Defense Advanced Research Projects Agency (DARPA) is gratefully acknowledged. The authors wish to express their gratitude to D. Steiner for helpful discussion on the theory of thermonuclear fusion reactions and to R. C. Block and C. D. West for suggesting improvements to this manuscript. They also wish to acknowledge the efforts made by the staff of the Institute of Mechanics of the Ufa-Bashkortostan Branch of the Russian Academy of Sciences, including I. Akhatov, R. Bolotnova, N. Vakhitova and A. Topolnikov, for their efforts in simulating the phenomena discussed in this paper.

REFERENCES

1 **Taleyarkhan, R., West, C., Cho, J. S., Lahey, R. T., Jr, Nigmatulin, R. I.** and **Block, R.** *Science*, 2002, **295**, 1868–1873.
2 **Taleyarkhan, R. P., Cho, J. S., West, C. D., Lahey R. T., Jr, Nigmatulin, R. I.** and **Block, R. C.** *Phys. Rev.–E*, 2004, **69**.
3 **Barber, B. P., Hiller, R., Arisaka, K., Fetterman, H.** and **Putterman, S. J.** *J. Acoust. Soc. Am.*, 1992, **91**, 3061.
4 **Barber, B., Wu, C. C., Lofstedt, R., Roberts, P. H.** and **Potterman, S. J.** *Phys. Rev. Lett.*, 1994, **72**, 1380.
5 **Crum, L.** and **Gaitan, D. F.** Frontiers of nonlinear acoustics. 12th International Symposium on *Nonlinear Acoustics*, 1990 (Elsevier Applied Science, New York).
6 **Crum, L.** and **Matula, T.** *Science*, 1997, **276**, 1348.
7 **Gaitan, D. F.** *Physics World*, 20 March 1999, **12**(3).
8 **Gaitan, D. F.** and **Crum, L. A.** *J. Acoust. Soc. Am. Suppl. 1*, 1990, **87**, 141.
9 **Gaitan, D. F., Crum, L. A., Church, C. C.** and **Roy, R. A.** *J. Acoust. Soc. Am.*, 1992, **91**, 3166.
10 **Hiller, R., Putterman, S.** and **Weninger, K.** *Phys. Rev. Lett.*, 1998, **80**, 1090.
11 **Kaiser, J.** *Sci. News*, 1995, **147**(17), 262.
12 **Lahey, R. T., Jr, Nigmatulin, R. I.** and **Taleyarkhan, R. P.** Proceedings of 3rd International Conference on *Transport Phenomena in Multiphase Systems*, Kielce, Poland, 2002.
13 **Lohse, D.** *Nature*, 1998, **392**, 21.
14 **McNamara, W. B., Didenko, Y. T.** and **Suslick, K. S.** *Nature*, 1999, **401**, 772.
15 **Metcalf, H.** *Science*, 1998, **279**, 1322.

16 **Moraga, F., Taleyarkhan, R. P.** and **Bonetto, F. J.** *Phys. Rev.*, 2000, **62**, 2233.
17 **Margulis, M. A.** *Phys. Sci. Adv.*, **170**(3), 263 (in Russian).
18 **Camara, C., Putterman, S.** and **Kirilov, E.** *Phys. Rev. Lett.*, 2004, **92**(12), 12430.
19 **Moss, W., Clarke, D., White, D.** and **Young, D.** *Phys. Fluids*, 1994, **6**(9), 2979.
20 **Moss, W., Clarke, D., White, D.** and **Young, D.** *Phys. Lett.*, 1996, **A211**, 69.
21 **Moss, W., Clarke, D.** and **Young, D.** *Science*, 1997, **276**, 1398.
22 **Nigmatulin, R. I., Akhatov, I. Sh., Vakhitova, N. K.** and **Lahey, R. T.** *Sonochemistry and Sonoluminescence* (Eds L. Crum *et al.*), NATO ASI Series, 1999, p. 127 (Kluwer Academic Publisher, Dordrecht/Boston/London).
23 **Brennen, C. E.** *Cavitation and Bubble Dynamics*, 1995 (Oxford University Press, New York).
24 **West, C. D.** and **Howlet, R.** *Nature*, 1967, **215**, 727.
25 **West, C. D.** and **Howlet, R.** *Br. J. Appl. Phys.*, 1968, **1**, 247.
26 **Delgadino, G., Bonetto, F.** and **Lahey, R. T., Jr** *Chem. Engng Commun.*, 2002, **189**, 786.
27 **Abramov, A. I., Kazansky, Yu. A.** and **Matusevich, E. S.** *Principles of Experimental Methods in Nuclear Physics* (in Russian), 1985 (Energoatomoizdat, Moscow).
28 **Knoll, G. F.** *Radiation Detection and Measurement*, 1989, (Wiley, New York).
29 **Harvey, J.** and **Hall, N.** *Nucl. Instrum. Meth. Phys. Res.*, 1979, **162**, 507.
30 **Lee, J. H.** and **Lee, C. S.** *Nucl. Instrum. and Meth. in Phys. Res.*, 1998, **A402**, 147.
31 **Hawkes, N. P., Adams, J. M., Dond, D. S., Jarvis, O. N.** and **Watkins, N.** *Nucl. Instrum. and Meth. in Phys. Res.,* 2002, A476, 190.
32 **Greenspan, M.** and **Tschiegg, C. E.** *J. Res. Nat. Bureau Stand.*, 1967, **4**(71C), 299.
33 **Hahn, B.** *Nuevo Cimento*, 1961, **22**, 650.
34 **Morch, K. A.** *Cavitation and Inhomogeneities in Underwater Acoustics* (Ed. W. Lauterborn), Springer Series—Electrophysics, 1980, Vol. 4, p. 95 (Springer, New York).
35 **Wang, Y. C.** and **Brennen, C. E.** Shock wave development in the collapse of a cloud of bubbles. *ASME FED, Cavitation and Multiphase Flows*, 1994, **194**, 15.
36 **Shapira, D.** and **Saltmarsh, M. J.** *Phys. Rev. Lett.*, **89**(10), 4302.
37 **Taleyarkhan, R. P., Block, R. C., West, C.** and **Lahey, R. T., Jr** Comments on Shapira/Saltmarsh paper (*htpp://www.rpi.edu/∼ laheyr/SciencePaper.pdf*).
38 **Lillie, R. A., Remel, I.** and **Gabriel, T. A.** Neutronic simulations of an acoustic cavitation (bubble fusion) experiment. ORNL/TM-2003/40, 2003.
39 **Zeldovich, Ya. B.** and **Raizer, Yu. P.** *Physics of Shock Waves and High-temperature Hydrodynamic Phenomena* (in Russian), 1963 (Nauka, Moscow).
40 **Nigmatulin, R. I.** *Dynamics of Multiphase Media* (in Russian), 1987, Vol. 1 (Nauka, Moscow); *Dynamics of Multiphase Media* (in English), 1991, Vol. 1 (Hemisphere, Washington–New York).
41 **Trunin, R. F.** *Chem. Phys.*, (11), 424 (in Russian).
42 **Nigmatulin, R. I., Akhatov, I., Bolotnova, R. K., Topolnikov, A. S., Vakhitova, N. K., Lahey Jr, R. T.** and **Taleyarkhan, R.I.** *Phys. Fluids*, 2004 (to be published).
43 **Gross, R. A.** *Fusion Energy*, 1984 (Wiley, New York).
44 **Bosch, H. S.** and **Hale, G. M.** *Nucl. Fusion,* 1992, **32**, 611.
45 **Paul, B.** *Rocket Engng*, 1962, (9), 3 (in Russian).
46 **Akhatov, I. Sh., Lindau, D., Topolnikov, A., Mettin, R., Vakhitova, H.** and **Lauterborn, N.** *Phys. Fluids*, 2001, **13**, 2805.
47 **Chodes, N., Warner, J.** and **Gagin, A.** *J. Atmos. Sci.*, 1974, **31**, 1351.
48 **Hagen, D. E., Schmitt, J., Trueblood, M., Carstens, J., White, D.** and **Aloff, D. J.** *J. Atmos. Sci.*, 1989, **46**, 803.
49 **Didenko, Y. T.** and **Suslick, K. S.** *Nature*, 2002, **418**, 394.
50 **Lohse, D.** *Nature*, 2002, **418**, 381.

